MARMARA UNIVERSITY

FACULTY OF ENGINEERING

AERODYNAMIC ANALYSIS OF EXTERNAL FUEL TANK IN JET AIRCRAFTS WITH ANSYS

Muhammed Emin DURKAN, Ömer Faruk SALMAN

GRADUATION PROJECT REPORT

Department of Mechanical Engineering

Supervisor

Doç.Dr. MUSTAFA YILMAZ

Table of Contents

Abstract

In this study, we aimed to enhance the operational duration and radius of supersonic combat aircraft by optimizing the aerodynamic performance of external fuel tanks, commonly known as drop tanks. We focused on reducing wave drag at 1.2 Mach and 10,000 ft, a major factor contributing to drag. To minimize wave drag, we utilized numerical designs of various nose cones used in rocketry, attempting shape optimization to ensure more effective mission performance.

Abbreviations

M = Mach Number

Re = Reynolds' Number

C_d = Drag Coefficient

C_{d_w} = Wave Drag Coefficient

$C_{d_{wv}}$ = Volume-Dependent Wave Drag Coefficient

$C_{d_{wl}}$ = Lift-Dependent Wave Drag Coefficient

F_d = Drag Force

A = Reference Area

ρ = Density

μ = Dynamic Viscosity

V = Velocity

CFD = Computational Fluid Dynamics

Introduction

In the intricate tapestry of military aviation, the operational range stands out as a paramount factor, dictating the strategic prowess and effectiveness of combat aircraft. This range, fundamentally, determines how far an aircraft can venture from its base to accomplish its mission and return safely without the need for mid-air refueling. In this context, a notable innovation that has significantly bolstered the combat radius of fighter jets is the integration of external fuel tanks, colloquially known as drop tanks. These supplementary units are pivotal in enabling aircraft to carry an amount of fuel far exceeding the limits of their internal structure, thereby markedly augmenting the aircraft's range and endurance. This capability is not just a matter of increased distance; it represents a profound enhancement of strategic flexibility and operational scope.

The primary aim and the driving impetus behind this comprehensive study is the meticulous optimization of the aerodynamic coefficients of these external fuel tanks. The rationale underpinning this endeavor is multifaceted. It is not merely about augmenting the fuel capacity; it is profoundly about engineering these tanks in such a manner that their integration results in minimal aerodynamic penalty. The presence of additional fuel should not inversely impact the aircraft's performance, agility, or fuel efficiency due to increased drag or weight. Therefore, the study is inherently about striking that delicate balance – maximizing fuel load while concurrently minimizing any resultant drag and performance loss, a balance that is crucial for maintaining the aircraft's combat effectiveness and operational efficiency.

The methodology adopted in this study was comprehensive and multi-faceted. It embarked on an exploratory journey, initiating with the precise determination of the aerodynamic coefficients of the fuel tank's initial design. This step was foundational, setting the stage for subsequent analyses and modifications. Recognizing the critical influence of aerodynamic factors such as wave drag and wake turbulence on an aircraft's efficiency, the study did not merely stop at measurement. It proactively explored significant design modifications aimed at mitigating these detrimental aerodynamic effects. This proactive approach ensured that every potential avenue for enhancement was explored and evaluated.

Furthermore, the study delved into the intricate dynamics of interference drag, focusing particularly on how the pylon – the structure that connects the drop tank to the aircraft – influences the overall aerodynamic performance of the system. This aspect is crucial, as the way the tank is attached can significantly affect the airflow around both the tank and the aircraft, potentially leading to increased drag. Understanding and optimizing this factor was key to ensuring that the benefits of increased fuel capacity did not come at an unacceptable cost in terms of performance.

The analysis was conducted under specific and controlled conditions – at an altitude of 10,000 ft and a velocity of 1.2 Mach. These conditions were not arbitrarily chosen; they represent a realistic operational envelope for many fighter aircraft, ensuring that the findings of

the study are relevant and applicable to real-world scenarios. This relevance is critical, as the main objective of this research is not merely academic insight but tangible, actionable improvements in military aviation.

The significance of this research extends beyond its immediate practical applications. It sets a benchmark for future aerodynamic innovations in aviation technology. By pushing the boundaries of what is possible in terms of fuel capacity and aerodynamic efficiency, this study contributes to the ongoing evolution of military aircraft, ensuring that they remain capable, versatile, and effective in the face of evolving challenges and threats.

Theoretical Background

Aerodynamics

Aerodynamics is a specialized field of fluid dynamics focusing on how air flows around objects, significantly influencing their movement and stability. At its core, it encompasses four primary forces: lift, weight, thrust, and drag. These forces interact to determine an object's trajectory, speed, and overall aerodynamic efficiency. Understanding and optimizing these forces are critical in various industries, particularly in designing aircraft, vehicles, and structures to ensure optimal performance and safety. Aerodynamic principles are not only pivotal in engineering but also play a significant role in environmental and energy-related applications.

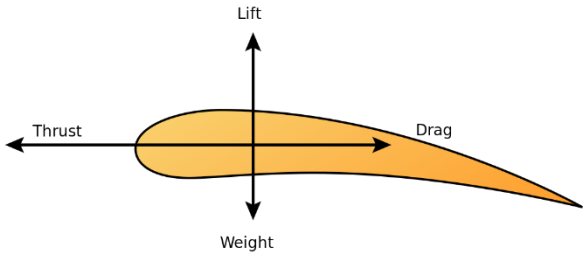

Figure 1 Aerodynamic Forces on an Airfoil

Drag and Drag Coefficient

Drag force is a physical force exerted by air on an aircraft in motion, opposing its direction of flight, while the drag coefficient quantifies this force relative to the aircraft's size and speed. Understanding and managing these are crucial for optimizing aircraft performance, especially in designing components like drop tanks, where efficiency against aerodynamic drag is a priority. The study of drag force and its coefficient has evolved significantly.

Initially rooted in basic observations, the field has grown into a sophisticated science underpinning modern aerodynamics, influencing aircraft design from the earliest biplanes to today's supersonic jets.

Drag is primarily caused by friction and pressure differences. Types of drag include parasitic drag (comprising form drag, skin friction, and interference drag) and induced drag. Each type has distinct characteristics and arises under different flight conditions.

The drag force (F_D) can be expressed mathematically as;

$$F_D = C_d A \frac{\rho V^2}{2}$$

The drag coefficient (C_d) is a dimensionless number that quantifies an object's resistance to fluid flow. It's influenced by factors like shape, airflow, surface roughness, and the Reynolds number.

Measuring drag involves wind tunnel testing and computational methods. Minimizing drag is crucial for enhancing fuel efficiency and performance. Techniques include streamlining shapes, using smooth surfaces, and optimizing lift-to-drag ratios. In designing drop tanks, considerations include minimizing their impact on the aircraft's overall drag. Balancing additional fuel capacity with aerodynamic efficiency is key.

Advancements in materials science, computational fluid dynamics, and aerodynamic theory continue to push the boundaries of efficiently managing drag force and the drag coefficient. This progress promises more fuel-efficient, faster, and environmentally friendly aircraft.

Wave Drag and Interference Drag

Understanding the intricacies of wave drag and interference drag is crucial for optimizing aircraft performance, especially at high speeds. These drag components, influenced by aircraft design and operational conditions, play pivotal roles in determining the overall aerodynamic efficiency and are integral considerations in the design and optimization of aircraft structures and components.

Wave Drag

Wave drag, often referred to as shock wave drag, becomes prevalent at supersonic airspeeds. This type of drag emerges when an obstacle, such as a wing's leading edge or a fuselage's nose, disrupts a supersonic airflow. The disturbance generates a shock wave, a thin layer of air wherein abrupt variations in flow parameters—pressure, temperature, density, speed, and Mach number—occur. As air passes through this shock wave, it typically experiences a sudden increase in density, pressure, and temperature, alongside a decrease in Mach number. The presence of shock waves reflects a significant transformation in the

airflow characteristics, leading to an increase in resistance against the aircraft's movement, known as wave drag.

Aircraft components, regardless of their simplicity or complexity, contribute to wave drag. Calculating the wave drag of an entire aircraft involves considering it as a single entity, rather than dissecting it into individual components. This method is empirical and approximative. The total wave drag coefficient (C_{d_w}) for an aircraft is primarily composed of volume-dependent wave drag ($C_{d_{wv}}$) and lift-dependent wave drag ($C_{d_{wl}}$). Volume-dependent wave drag, a function of the aircraft's volume, significantly surpasses lift-dependent wave drag.

Interference Drag

Interference drag arises when different parts of an aircraft, such as the engine nacelle and the rear pylon, are placed in proximity to each other. This drag is especially challenging to calculate accurately due to the complex interactions between the various components. Examples include the drag created by placing an engine nacelle near a rear pylon, the interaction between the wing and fuselage in a mid-wing configuration, the effect of a horizontal tail positioned aft of a jet engine exhaust nozzle, and the impact of a wing's leading edge positioned aft of a propeller wake.

One common manifestation of interference drag is observed at the junction where a wing attaches to a fuselage. At this point, the boundary layers from the wing and fuselage interact and locally thicken, increasing drag. This drag penalty is exacerbated under certain configurations and is vividly depicted in the documentation where wing-fuselage interference drag is graphically represented.

Mach Number

The relationship between the aircraft's velocity and the speed of sound in the surrounding gas dictates the extent of various compressibility effects. Recognizing the significance of this velocity ratio, aerodynamic experts have denoted it using a specific parameter known as the Mach number, in tribute to Ernst Mach, a physicist from the late 19th century who delved into the study of gas dynamics. The Mach number, denoted as M, enables us to establish different flight regimes where the impact of compressibility effects varies.

1. Subsonic Speed: Speeds below the speed of sound (Mach 1 or less). Sound waves travel faster than the aircraft at subsonic speeds. Compressibility effects are typically negligible and drag is relatively low.
2. Transonic Speed: Speeds near the speed of sound, typically around Mach 0.8 to 1.2. Aircraft at transonic speeds experience both subsonic and supersonic airflow regions. Compressibility effects become significant, leading to potential increases in drag.

3. Supersonic Speed: Speeds above the speed of sound (Mach 1 to 5). Supersonic aircraft generate shockwaves as they move, and compressibility effects are important for design considerations. Aerodynamic heating is also a factor at high supersonic speeds.
4. High Supersonic Speed: Speeds ranging from Mach 3 to 5. At these velocities, shockwaves and compressibility effects are more pronounced, requiring advanced engineering solutions for aircraft and vehicle design.
5. Hypersonic Speed: Speeds exceeding five times the speed of sound (Mach 5 or higher). Hypersonic vehicles experience extreme aerodynamic conditions, including significant heating due to air friction and the need to consider chemical reactions in the atmosphere. Hypersonic flight presents unique challenges in terms of design and engineering.

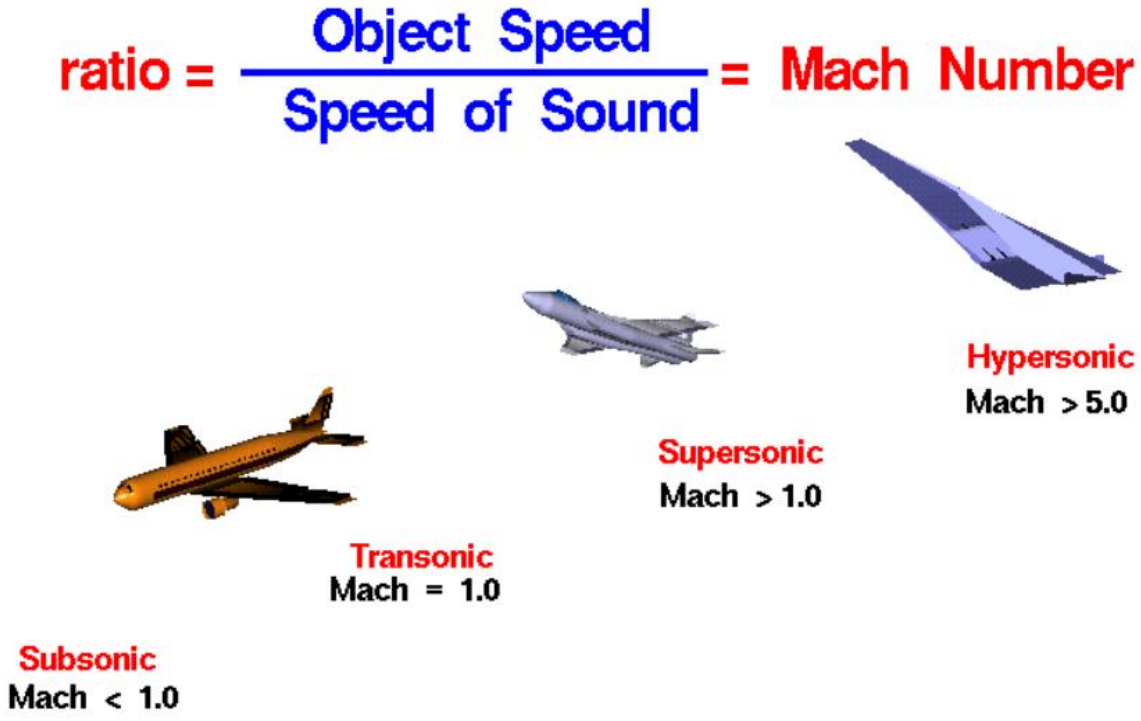

Compressible Flow

Compressible flow refers to the behavior of gases when they are subjected to varying conditions such as changes in pressure, temperature, and velocity. In these scenarios, the density of the gas can change significantly, distinguishing it from incompressible flow where density is assumed to be constant.

In the realm of aerodynamics, understanding compressible flow is crucial, especially at high speeds. As an aircraft's speed approaches and surpasses the speed of sound, the assumptions of incompressible flow no longer hold true. Parameters like the Mach number, which represents the ratio of the object's speed to the speed of sound in the surrounding medium, and the Reynolds number, indicative of the flow regime and inertia vs. viscous forces, become pivotal.

Compressible flow principles are integral to the design and operation of high-speed aircraft, rockets, and spacecraft. Engineers must account for varying air density, temperature, and pressure to optimize performance, stability, and fuel efficiency.

Shockwaves

Shockwaves are abrupt changes in pressure, temperature, and density, occurring when an object moves through a medium at a speed exceeding the speed of sound in that medium.

- *Normal Shockwaves:* Occur perpendicular to the flow direction. They significantly decelerate the flow, increasing pressure and temperature.
- *Oblique Shockwaves:* Occur from an angle to the flow direction. They are weaker than normal shocks but can still cause considerable changes in flow properties.

Shockwaves are associated with increased drag (wave drag), structural loads, and can lead to phenomena such as sonic booms. They present significant challenges in aircraft design, particularly in supersonic and hypersonic regimes.

Oblique Shock

An oblique shock is a type of shockwave that forms at an angle in the direction of flow. Unlike normal shocks, oblique shocks do not completely halt the flow but change their direction and properties like velocity, temperature, and pressure.

When interacting with aerodynamic surfaces, oblique shocks can induce changes in lift and drag forces, alter stability characteristics, and affect control surface effectiveness. Designers must carefully consider these effects, especially in high-speed aircraft.

Incorporating knowledge about oblique shocks allows for optimized wing and fuselage shapes, minimizing drag and structural stress.

Computational Fluid Dynamics (CFD)

In this project, we will use CFD methods. Under the title of CFD Applications, we will use Ansys Fluent for preprocessing, setup, and solution and postprocessing. CFD is the theoretical method to analyze fluid flow. This method is relatively reliable and of course cheaper than the experimental methods.

Limitations of Flow Analysis

1. Mach number is 1.2.
2. Aircraft altitude => 10000 ft

What is Computational Fluid Dynamics?

Computational Fluid Dynamics (CFD) is a multifaceted field, integrating mathematics, physics, and computer science to analyze fluid flow behaviors. This branch of fluid mechanics utilizes numerical methods and algorithms to solve and analyze problems involving fluid flows, simulating the interaction of gases and liquids with various surfaces under a wide range of conditions.

CFD's core involves discretizing a fluid domain into small, manageable elements, forming a mesh. The physical behavior of the fluid is governed by the Navier-Stokes equations, which, due to their complexity, are often impossible to solve analytically for real-world problems. CFD overcomes this by applying numerical methods to solve these equations within each element of the mesh, iterating towards a solution that describes the velocity, pressure, and other properties of the fluid throughout the domain.

The applications of CFD are vast, ranging from predicting weather patterns and understanding environmental phenomena to designing high-performance cars and aircraft. In engineering, CFD is indispensable for analyzing aerodynamic performance, optimizing HVAC systems for energy efficiency, and even in the medical field for simulating blood flow in arteries.

The power of CFD also brings challenges. The accuracy of a CFD simulation critically depends on the quality of the mesh, the appropriateness of the turbulence model, and the precision of the boundary conditions set for the simulation. Moreover, CFD computations are resource-intensive, requiring high-performance computing systems for complex simulations. Despite these challenges, the continuous advancement in computational power and numerical methods is expanding the capabilities and applications of CFD, making it an increasingly valuable tool in scientific research and engineering design.

We need the ability to predict and control fluid dynamics. CFD is one of the main tools that we use for this. Most of projects for fluid are done with 3 different approaches analytical, computational, and experimental.

Analytical Approach

Analytical approach, on the other hand, is a method that can sit and calculate results by hand or with a calculator. Unfortunately, it is not a valid method for most complex situations.

Computational Approach

We mentioned most cases can't be solved by analytical methods, but we can use numerical methods with appropriate solution domain with help of computers computational analysis can be done also cheaper and more flexible method compared to experiments.

Experimental Approach

More accurate than computational methods but also limited and expensive. Needs special facilities and equipment. There is a high construction cost and need well calibrated equipment.

As we see Fluid dynamics very complicated and hard area to understand different conditions of fluids there is a joke about this concept. Nearly impossible to come up with a solution to consider all physical effects. The full equation for fluid dynamics is what we call the Navier Stokes equations. There is no general analytical solution to solve this equation. So, we must turn to the computational method to find solutions.

Navier Stokes Equations

The Navier-Stokes Equations are a set of partial differential equations that describe the motion of viscous fluid substances. These equations are central to fluid mechanics, capturing the essence of fluid flow by accounting for various forces acting on the fluid elements. The equations consist of the continuity equation (for mass conservation), the momentum equation (describing the force balance), and the energy equation (for energy conservation). Solving these equations provides insights into the velocity, pressure, and density fields within the fluid. Despite their comprehensive nature, finding analytical solutions to the Navier-Stokes Equations is often challenging due to their complexity, especially for turbulent or three-dimensional flows. As a result, numerical methods, and computational fluid dynamics (CFD) are typically employed to obtain approximate solutions, playing a crucial role in various applications, from engineering design to meteorology and oceanography. The Navier-Stokes Equations, therefore, are not just mathematical expressions but tools that bridge theory and practical applications, providing a window into the complex and beautiful dynamics of fluids.

Navier stokes equations can be solved by computers and these equations are made up of 4 equations continuum and 3 momentum equations mostly. These equations are performed with basics objects like a box. Computational methods use these equations by dividing the geometry into simple elements called mesh and computer solve these equations iteratively. It should be known that these equations can differ between incompressible flow and compressible flow. The steps are listed as the following:

1. Divide your object into millions of tiny little boxes (meshes)
2. Each cell interacts with its neighbors.
3. Engineers set known values for the boundaries.
4. Computer iterates to balance all the cells and the edge boundaries.

Up to this point, we have given brief information about the methods of examining the behavior of fluids and CFD. At this point, we will state the advantages and disadvantages of the CFD method.

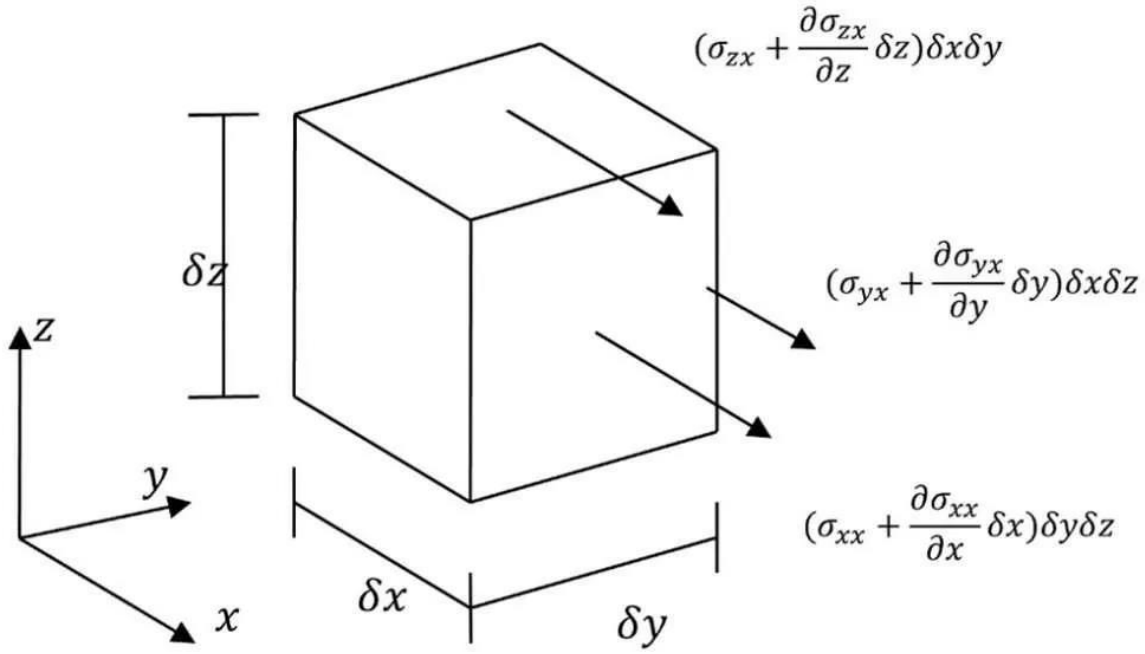

Advantages of CFD

- **Precision:** Enables accurate predictions of fluid flow behavior.
- **Versatility:** Applicable to a vast range of industries and problems.
- **Cost-Effective:** Reduces the need for physical prototypes.
- **Risk-Free:** Allows for the simulation of dangerous scenarios without real-world risks.
- **Customization:** Parameters can be easily altered to study various scenarios.
- **Efficiency:** Streamlines the design and development process.
- **Iterative Analysis:** Facilitates rapid testing of design modifications.
- **Scalability:** Suitable for problems of different sizes and complexities.

Disadvantages of CFD

- **Resource Intensive:** Requires significant computational power and time.
- **Expertise Required:** Demands in-depth knowledge of fluid dynamics and numerical methods.
- **Model Dependency:** Solutions are only as accurate as the models and assumptions.
- **Data Sensitivity:** Highly sensitive to initial and boundary conditions.
- **Validation Requirement:** Results need to be validated against experimental data.
- **Over-reliance Risk:** Can lead to overlooking practical considerations if overly relied upon.
- **Software Costs:** High-quality CFD software can be expensive.
- **Meshing Complexity:** Creating an optimal mesh can be challenging and time-consuming.

We said that CFD is a numerical method. There are two ways to know how our solution is correct:

- Validation studies
- Mesh independence studies

What is Mesh?

In CFD, a mesh is a network of elements (nodes, edges, faces) used to discretize the computational domain. Each element provides a local approximation of the geometry and solution field. Mesh elements can be tetrahedra, hexahedra, prisms, or pyramids, each with its suitability based on the geometry and physics of the problem. A well-designed mesh captures important flow features and geometry details while balancing computational efficiency. Mesh quality, in terms of element shape and size distribution, directly influences the accuracy and stability of CFD simulations.

Mesh Independence Index

The Mesh Independence Index (MII) in Computational Fluid Dynamics (CFD) is a crucial metric used to ascertain the reliability and accuracy of simulation results. It is fundamentally about ensuring that the numerical results of a CFD simulation have converged to a solution that is independent of the mesh used in the computation. The mesh in CFD is a discretization of the computational domain into small, finite elements or volumes, over which the governing equations (such as Navier-Stokes equations for fluid dynamics) are solved.

Achieving mesh independence typically involves a systematic process:

1. **Initial Coarse Mesh Simulation:** The process starts with a simulation using a relatively coarse mesh. This initial solution provides a baseline but is generally not accurate enough for final analysis.
2. **Progressive Mesh Refinement:** The mesh is refined, often by reducing the size of the mesh elements, thereby increasing the number of elements. This refinement process is not arbitrary but is usually guided by parameters like the aspect ratio, skewness, and gradient of the solution variables.
3. **Solution Monitoring:** After each refinement, the simulation is re-run, and key parameters (like velocity profiles, pressure distribution, or temperature gradients) are monitored. The results of these parameters are compared between the current and previous mesh refinements.
4. **Convergence Criterion:** The process of refinement continues until the changes in the monitored parameters between successive meshes fall below a predefined threshold. This threshold is often a small percentage change and is determined based on the required precision for the study or industry standards.
5. **Validation and Analysis:** Once mesh independence is achieved, the results can be considered reliable for that mesh refinement. However, it's also crucial to validate these results with experimental data or theoretical predictions to ensure that the model accurately represents the physical phenomena.
6. **Computational Efficiency:** While finer meshes typically provide more accurate results, they also require more computational resources and time. Hence, there's a trade-off between the level of detail in the mesh and the computational cost. The optimal mesh is the one that provides sufficiently accurate results with the lowest computational expense.
7. **Quality over Quantity:** It's worth noting that having a higher number of elements doesn't automatically translate to better results. The quality of the mesh, meaning how well the mesh elements conform to the geometry and flow features of the model, is equally important.

In summary, the Mesh Independence Index is an essential concept in CFD that ensures the reliability of simulation results by confirming that these results are independent of the mesh used. It's a balance between computational efficiency and the accuracy of the results, and it's a critical step in the CFD simulation process to validate the model's predictive capability.

Methodology

As stated in the introduction, the aim of the project is to reduce the drag coefficient in external fuel tanks. These external fuel tanks will be designed for high-performance supersonic aircraft. The suitable analysis speed for the designed fuel tanks is determined as 1.2 Mach, and the altitude is set at 10,000 ft. The process of selecting the optimal design proceeded as follows throughout the study:

1- Designing the main model and determining the Cd coefficient.
2- Mathematical modeling of the parts to be improved.
3- Selection of a nose cone suitable for environmental conditions.
4- Generating the points of the cone using Excel.
5- Preparing the tank geometry and volume of flow with the SolidWorks program.
6- Calculating the Cd coefficient using Ansys Fluent.

Used Software

Excel

Excel is a highly useful tool for numerical calculations, data management, and analysis. It operates in a spreadsheet format, providing users with a platform to organize, calculate, and visualize large volumes of data. It is widely used in projects, businesses, and for personal purposes.

Excel simplifies mathematical operations by allowing users to use formulas and functions. Additionally, it facilitates better understanding of data by creating charts and graphs. It finds application in various fields, such as projects, data analysis, or financial forecasting. Just like in your project, Excel enables quick and accurate calculations of data like x and y coordinates. Excel's flexibility and user-friendliness make it a preferred tool for data processing needs across many domains.

SolidWorks

SolidWorks is professional software used for three-dimensional (3D) modeling and engineering design. This software enables engineers and designers to create complex parts and assemblies, perform analyses, generate simulations, and produce detailed technical drawings for products. SolidWorks is widely used in various fields such as industrial design, mechanical engineering, electrical engineering, and architecture.

Ansys Fluent

Ansys Fluent is a software used for computational fluid dynamics (CFD) simulations, which are computer-based numerical simulations of fluid flow and related phenomena. This software provides a powerful tool for engineers and scientists to model and analyze fluid dynamics, heat transfer, chemical reactions, and other physical processes. Ansys Fluent is widely preferred for solving complex fluid dynamics problems in various fields such as industrial design, aerospace, automotive, energy, thermal management, and many others.

Key functions of Ansys Fluent include simulating fluid motion, temperature distribution, pressure changes, and other fluid behaviors. It is used to make improvements in

product and system designs, optimize performance, and expedite the design process. Additionally, it assists in making design decisions by studying fluid behavior under different conditions. Ansys Fluent is renowned as a powerful tool for solving complex engineering problems.

Nose Cone Geometry

In the introduction section, we mentioned that wave drag is a significant factor in supersonic flows, and engineers have developed various methods to cope with this phenomenon. One of these methods is optimizing the geometry, where typically ogive shapes are preferred for fuel tanks and many other applications. However, in our study, we reached a solution through trial and error on the nose cone geometry. The figure provides a performance comparison of different nose geometries at various Mach speeds.

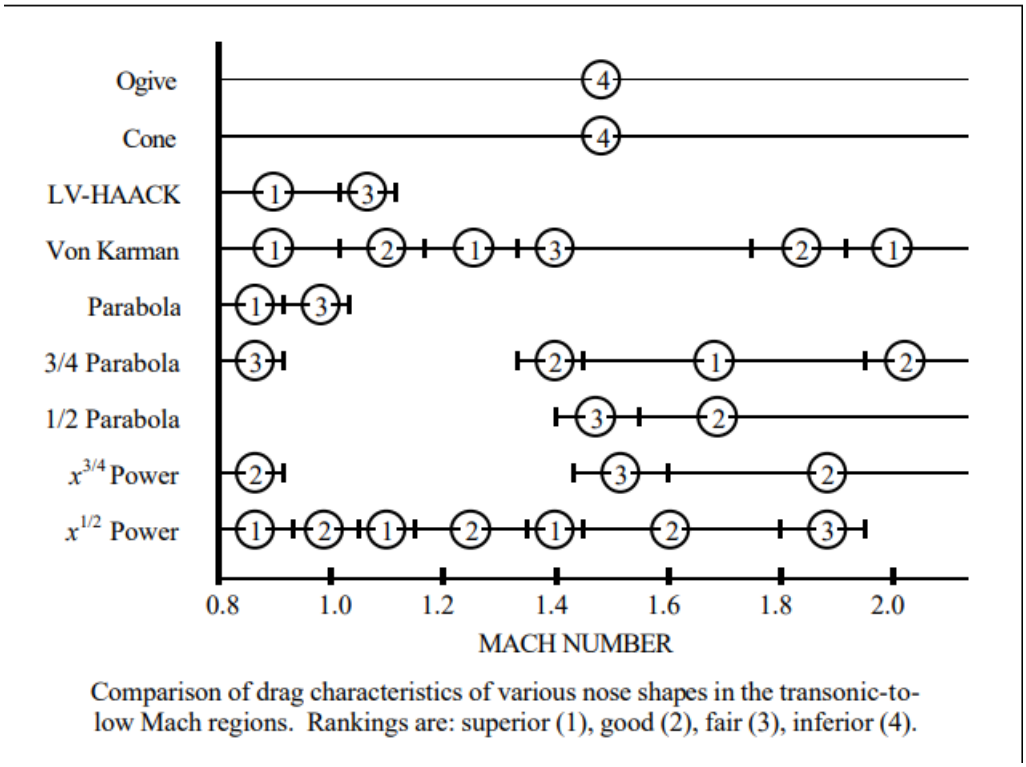

Comparison of drag characteristics of various nose shapes in the transonic-to-low Mach regions. Rankings are: superior (1), good (2), fair (3), inferior (4).

Figure 2: Nose Cone Geometry v Mach

As seen in the figure, the nose cone geometries that appear suitable for our flight speeds are the Von Karman (a special structure within the Haack series) and the power series. These geometries were originally developed for rocketry models. Although the Von Karman model from the Haack series appears to be the most suitable, it has a sharper geometry, which reduces the amount of fuel to be carried. Nevertheless, we also experimented with Haack series geometries and included them in our study.

Secondly, at a Mach speed of 1.2, the Power Series stands out. The Power Series offers a design that can be either sharper or blunter according to the designer's preference. In

the following sections, detailed information and formulas about these structures will be provided.

General Dimensions

In all the equations provided for nosecone shapes, we use certain variables to describe geometry. L represents the total length of the nosecone, while R represents the radius of the base of the nosecone. The variable y represents the radius at any point x along the nosecone's length, which varies from 0 at the tip of the nosecone to L. These equations define the 2-dimensional profile of the nose shape. To create the complete 3-dimensional nosecone, we rotate this profile around the centerline, denoted as C/L. It's important to note that these equations describe the 'ideal' or 'perfect' nosecone shape. In practice, nosecones are often modified, either blunted or truncated, for manufacturing or aerodynamic considerations.

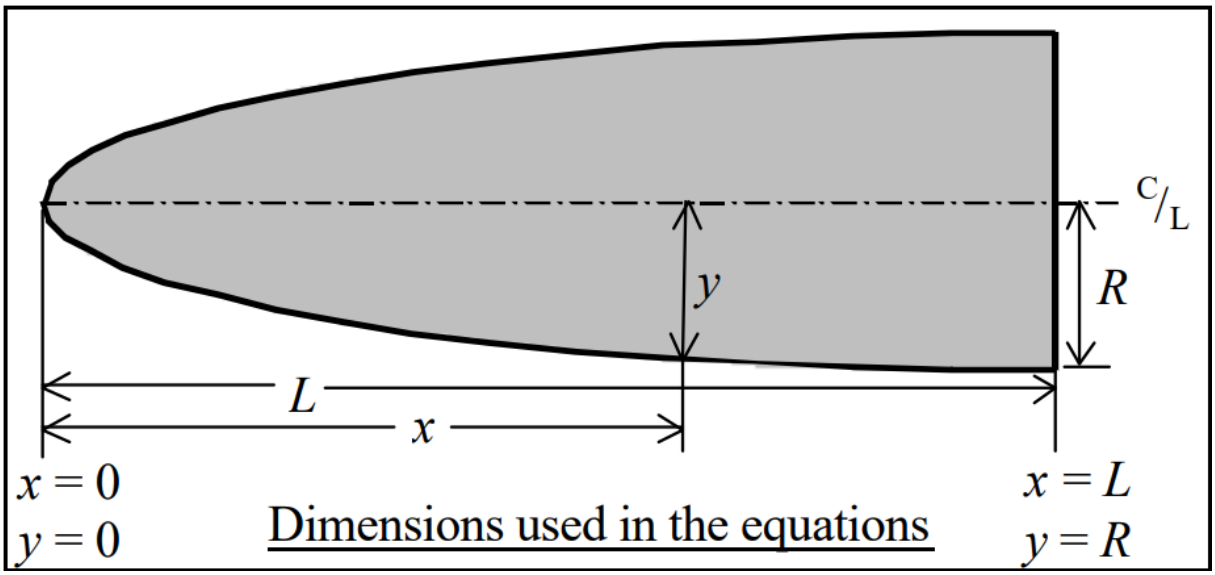

Figure 3: Nose Cone General Dimensions

Power Series

The Power Series includes a nose cone shape that is often referred to as 'parabolic' by modelers, although it's interesting to note that the actual parabolic nose cone belongs to a different category known as the Parabolic Series. The distinguishing features of the Power Series shape are its typically blunt tip and the fact that its base does not align smoothly with the body tube. There is always a noticeable discontinuity at the joint where the nosecone meets the body, which doesn't appear very aerodynamic. However, sometimes modifications are made at the base to improve this transition. It's worth mentioning that people often mistakenly refer to it as a parabolic shape when they are seeking an elliptical shape, which has a smooth base alignment. It's also noteworthy that both a flat-faced cylinder and a cone are shapes belonging to the Power Series. The Power Series nose shape is created by rotating a

parabola around its axis, with the base of the nosecone parallel to the latus rectum of the parabola. The 'n' factor determines the 'bluntness' of the shape; as 'n' decreases towards zero, the Power Series nose shape becomes increasingly blunt, while values of 'n' above about 0.7 result in a sharper tip.

For $0 \le n \le 1$, $$y = R\left(\frac{x}{L}\right)^n$$

Where: $n = 1$ for a **CONE**
$n = .75$ for a **¾POWER**
$n = .5$ for a **½POWER (PARABOLA)**
$n = 0$ for a **CYLINDER**

HAACK Series

Haack Series shapes are not based on geometric figures but are instead derived mathematically to minimize drag. This series consists of a continuous range of shapes determined by the value of 'C' in the equations provided below. Within this series, two specific values of 'C' hold particular significance. When 'C' equals 0, it is denoted as 'LD,' representing the configuration that minimizes drag for a given length and diameter. On the other hand, when 'C' equals 1/3, it is indicated as 'LV,' signifying the shape that minimizes drag for a given length and volume. It's important to note that Haack series nose cones do not have a perfectly smooth transition to the body at their base, but this discontinuity is usually so minimal that it's hardly noticeable. Similarly, Haack nose tips are not sharply pointed; they have a slight rounding.

$$\theta = \cos^{-1}\left(1 - \frac{2x}{L}\right) \qquad y = \frac{R\sqrt{\theta - \frac{\sin(2\theta)}{2} + C\sin^3\theta}}{\sqrt{\pi}}$$

Where: $C = 1/3$ for **LV-HAACK**
$C = 0$ for **LD-HAACK** (This shape is also known as the **Von Karman**, or, the **Von Karman Ogive**)

Using the formulas provided above and Excel, seven different tank geometries were obtained, and these geometries were created based on the variable "L" as shown in the figure. As an example, the lengths of various fighter aircraft tanks were used; however, it should be noted that these dimensions are not specified by authorities. The tanks were selected to have

volumes equivalent to 300 gallons, with the first tank being 6 meters in length and 0.6 meters in diameter, and the second tank being 4 meters in length and 0.8 meters in diameter.

Geometry Tables

Power Series

For obtain blunt geometry we choose n=0.5.

$$n = 0.5 \;\; y = R\left(\frac{x}{L}\right)^{0.5}$$

To Excel formula for 1m L (0,30*(E3/D3) ^ (0,5)) same goes for other geometries.

For L =1 and 6m total length 0.5 Power Series

x	y	mm
0	0	0
0,10	0,10119	101,193
0,20	0,14311	143,108
0,30	0,17527	175,271
0,40	0,20239	202,386
0,50	0,22627	226,274
0,60	0,24787	247,871
0,70	0,26773	267,731
0,80	0,28622	286,217
0,90	0,30358	303,579
1,00	0,32	320
1,10	0,33562	335,619
1,20	0,35054	350,542
1,30	0,36486	364,856
1,40	0,37863	378,629
1,50	0,39192	391,918

For L=0.75 and 6m total length 0.5 Power Series

x	y	mm
0	0	0
0,1	0,11685	116,847
0,2	0,16525	165,247
0,3	0,20239	202,386
0,4	0,23369	233,695
0,5	0,26128	261,279
0,6	0,28622	286,217
0,7	0,30915	309,149
0,8	0,33049	330,495
0,9	0,35054	350,542
1	0,3695	369,504
1,1	0,38754	387,539
1,2	0,40477	404,772
1,3	0,4213	421,3
1,4	0,4372	437,203
1,5	0,45255	452,548

For L=1.2 and 6m total length 0.5 power Series

x	y	mm
0	0	0
0,1	0,09238	92,376
0,2	0,13064	130,639
0,3	0,16	160
0,4	0,18475	184,752
0,5	0,20656	206,559
0,6	0,22627	226,274
0,7	0,2444	244,404
0,8	0,26128	261,279
0,9	0,27713	277,128
1	0,29212	292,119
1,1	0,30638	306,377
1,2	0,32	320

For L=1.5 and 6m total length 0.5 Power Series

x	y	mm
0	0	0
0,10	0,08262	82,6236
0,20	0,11685	116,847
0,30	0,14311	143,108
0,40	0,16525	165,247
0,50	0,18475	184,752
0,60	0,20239	202,386
0,70	0,2186	218,602
0,80	0,23369	233,695
0,90	0,24787	247,871
1,00	0,26128	261,279
1,10	0,27403	274,032
1,20	0,28622	286,217
1,30	0,2979	297,904
1,40	0,30915	309,149
1,50	0,32	320

The total length indicated in the tables above was intended for the 6-meter tanks included in the Power Series analysis. However, when creating the nose cones for the 4-meter tanks, we used 2 different "L" values based on the results of the above analyses. Nevertheless, to maintain the report's structure, we will also provide the spreadsheets for the 4-meter tanks under this heading.

For L=1 and 4m total length 0.5 Power Series

x	y	mm
0	0	0
0,10	0,12649	126,491
0,20	0,17889	178,885
0,30	0,21909	219,089
0,40	0,25298	252,982
0,50	0,28284	282,843
0,60	0,30984	309,839
0,70	0,33466	334,664
0,80	0,35777	357,771
0,90	0,37947	379,473
1,00	0,4	400

For L= and 4m total length 0.5 Power Series

x	y	mm
0	0	0
0,1	0,14606	146,059
0,2	0,20656	206,559
0,3	0,25298	252,982
0,4	0,29212	292,119
0,5	0,3266	326,599
0,6	0,35777	357,771
0,7	0,38644	386,437
0,8	0,41312	413,118
0,9	0,43818	438,178
1	0,46188	461,88
1,1	0,48442	484,424
1,2	0,50596	505,964

HAACK Series

For L=1 and 4m total length

x	teta	sin(2teta)/2	y
100	0,522315	0,4323693	54,14583
200	0,747584	0,4985708	90,0921
300	0,927295	0,48	120,7459
400	1,085278	0,4127355	148,0591
500	1,230959	0,3142697	172,8568
600	1,369438	0,1959592	195,5748
700	1,50408	0,0665184	216,4654
800	1,637512	-0,0665184	235,6752
900	1,772154	-0,1959592	253,2796
1000	1,910633	-0,3142697	269,2965
1100	2,056314	-0,4127355	283,6875
1200	2,214297	-0,48	296,3453
1300	2,394008	-0,4985708	307,0562
1400	2,619278	-0,4323693	315,386
1500	3,141593	-1,225E-16	320,0001

For L= and 4m total length

x	teta	sin(2teta)/2	y
100	0,643501	0,48	73,00214
200	0,927295	0,48	120,7459
300	1,159279	0,3666061	160,7394
400	1,369438	0,1959592	195,5748
500	1,570796	6,126E-17	226,2743
600	1,772154	-0,1959592	253,2796
700	1,982313	-0,3666061	276,7001
800	2,214297	-0,48	296,3453
900	2,498092	-0,48	311,5618
1000	3,141593	-1,225E-16	320,0001

Mesh Independence Index Table

Mesh Number (Million)	Max. Pressure (Pa)
1.023	$1.547x10^5$
1.222	$1.501x10^5$
1.847	$1.500x10^5$
2.094	$1.499x10^5$

The error between the last two rows in the table is less than 1%, therefore an acceptable mesh count for the solution has been determined as 1.847 million meshes.

Pre-Process Details

Domain

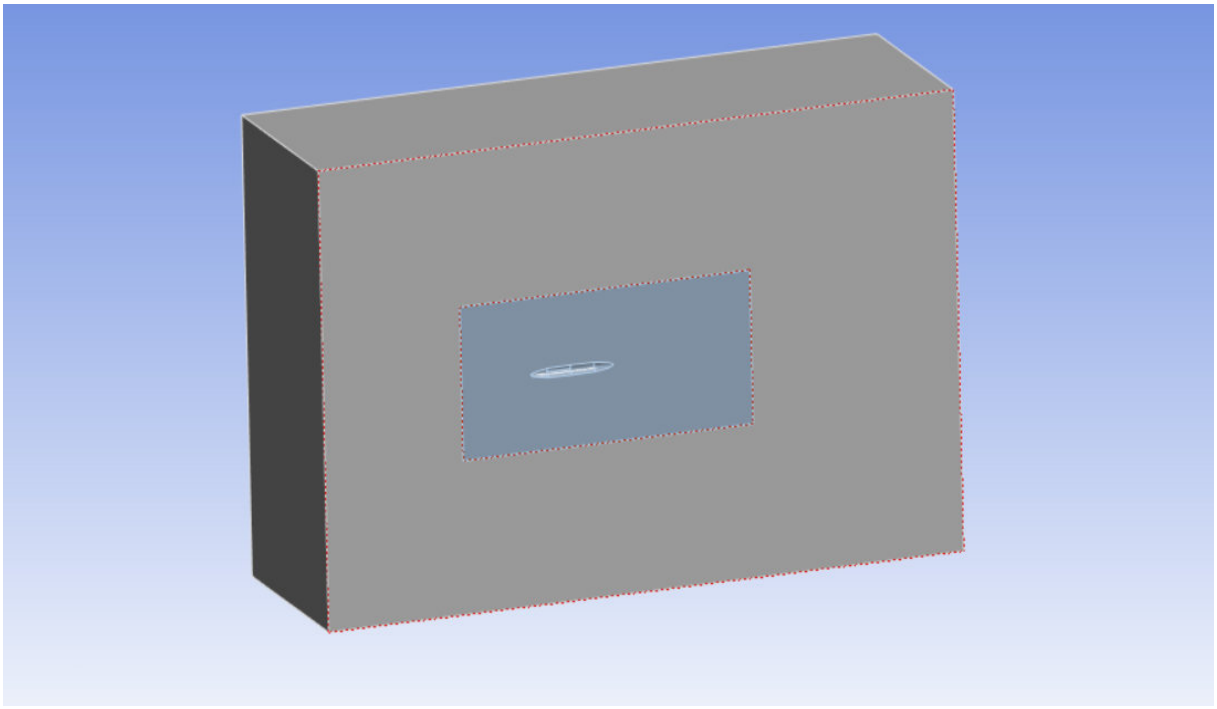

Figure 4: Drop Tank Domain

Domain Details

The visible face of the tank forms our symmetrical face, with a horizontal extent of 46 meters, a vertical extent of 30 meters, and a depth of 15 meters, considering symmetry, the extent is 30 meters. The domain was created with Body 2, while a smaller body, shown in blue in the image, was created at the nose and tail of the tank to assign a finer mesh in the areas closer to the walls for insignificant parts of the analysis. This was done with the aim of creating a more robust mesh network with fewer mesh elements.

Mesh Details

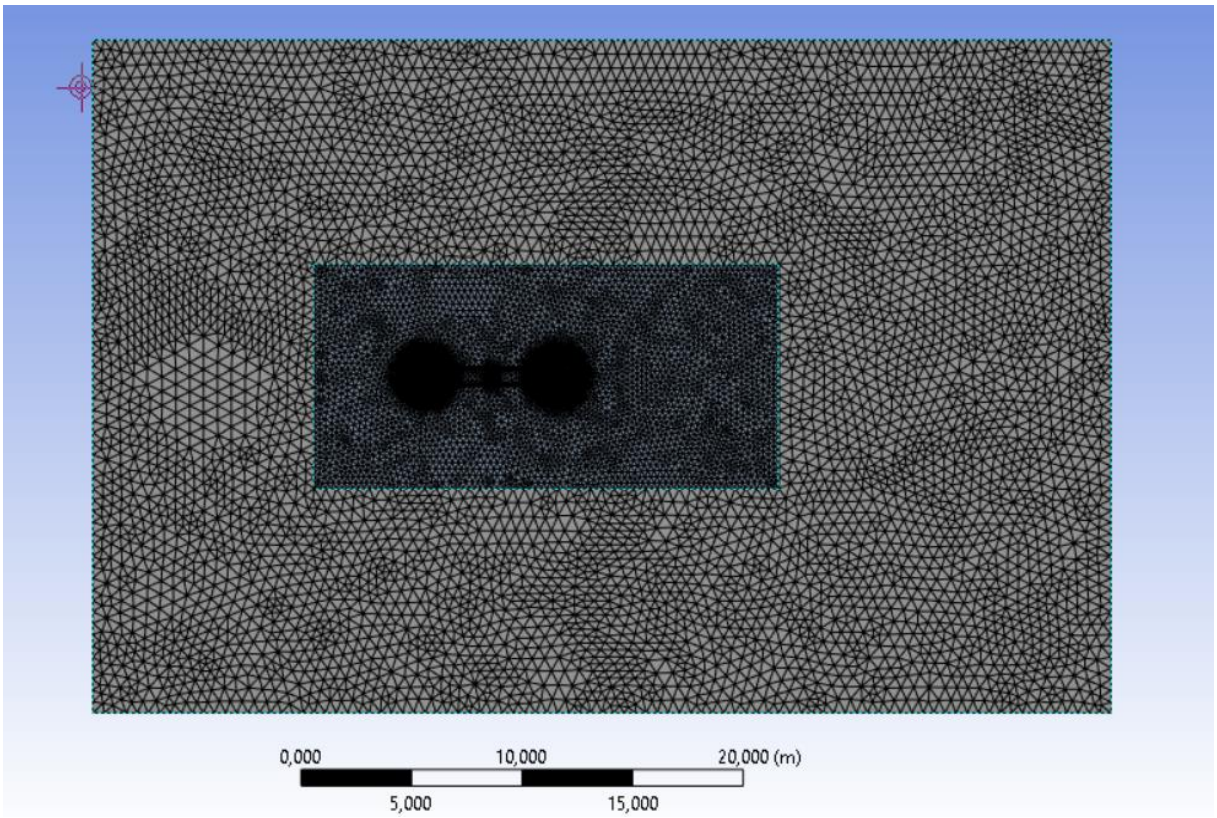

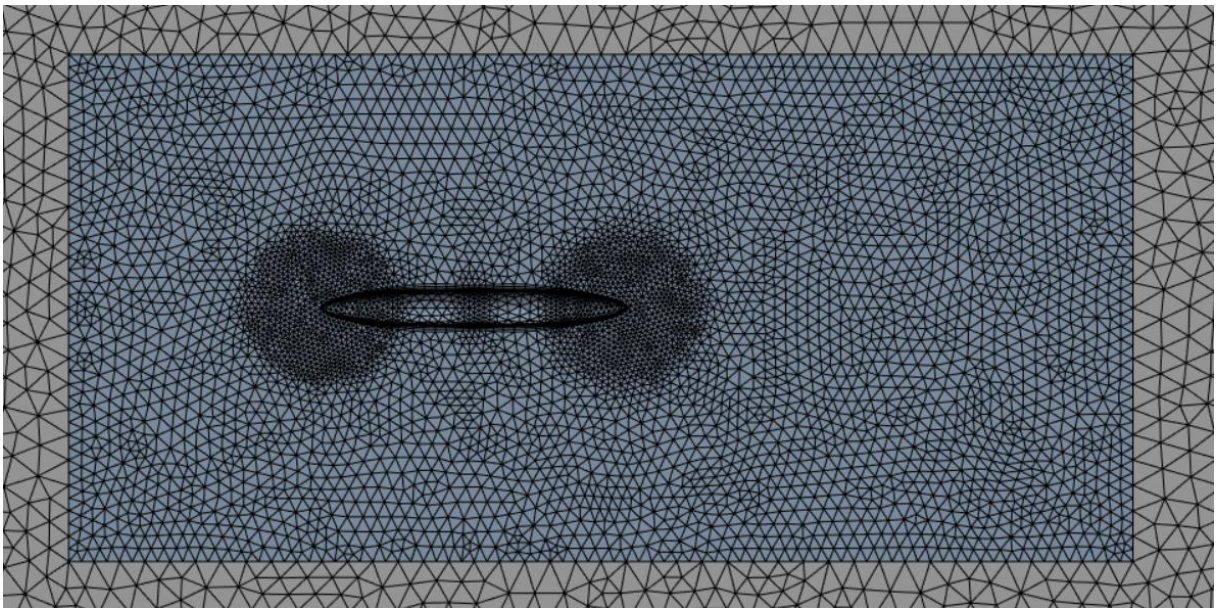

Global Mesh Settings

Display	
Display Style	Use Geometry Setting
Defaults	
Physics Preference	CFD
Solver Preference	Fluent
Element Order	Linear
Element Size	0,5 m
Export Format	Standard
Export Preview Surface Mesh	No
Sizing	
Use Adaptive Sizing	No
Growth Rate	Default (1,2)
Max Size	Default (1, m)
Mesh Defeaturing	Yes
Defeature Size	Default (2,5e-003 m)
Capture Curvature	Yes
Curvature Min Size	Default (5,e-003 m)
Curvature Normal Angle	Default (18,°)
Capture Proximity	No
Bounding Box Diagonal	56,93 m
Average Surface Area	276,44 m²
Minimum Edge Length	0,47124 m

Global mesh settings also apply to the larger body seen in the domain section.

Inflation

Inflation layers, a technique also known as boundary layer mesh refinement, involves adding additional layers of mesh elements near walls in CFD (Computational Fluid Dynamics) simulations. To create inflation layers, we need to determine y^+, which is a dimensionless wall distance parameter used in CFD. It represents the distance from a wall to the first computational node in a simulation. With the given conditions, we calculated the wall spacing for the desired y^+ = 1, which was computed as 0.0000014081312819 meters. The Reynolds number (Re) was computed as Re = 20750577.646138374. There's no need to mention that these conditions indicate turbulent flow.

Local Mesh Settings

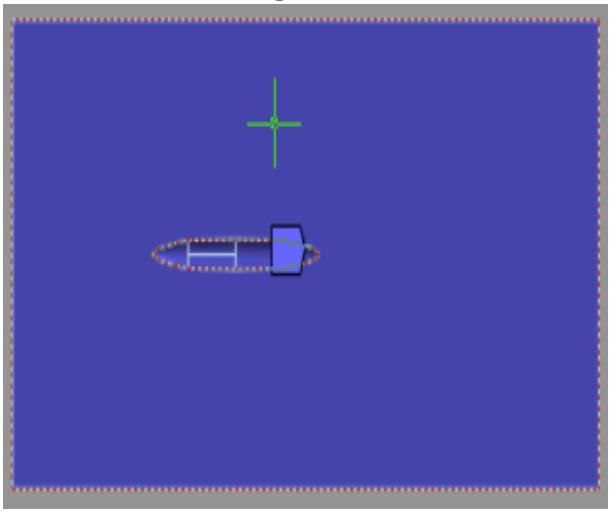

Figure 5: Body Sizing

Details of "Body Sizing 2" - Sizing	
Scope	
Scoping Method	Geometry Selection
Geometry	1 Body
Definition	
Suppressed	No
Type	Element Size
Element Size	0,2 m
Advanced	
Defeature Size	Default (2,5e-003 m)
Growth Rate	Default (1,2)
Capture Curvature	Yes
Curvature Normal Angle	Default (18,°)
Local Min Size	Default (5,e-003 m)
Capture Proximity	No

Figure 6: Body Sizing Details

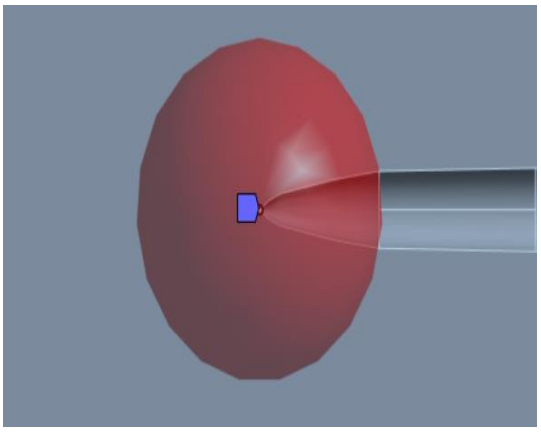

Figure 7: Vertex Sizing

Details of "Vertex Sizing" - Sizing	
Scope	
Scoping Method	Geometry Selection
Geometry	1 Vertex
Definition	
Suppressed	No
Type	Sphere of Influence
Sphere Radius	1,35 m
Element Size	0,1 m

Figure 8: Vertex Sizing Details

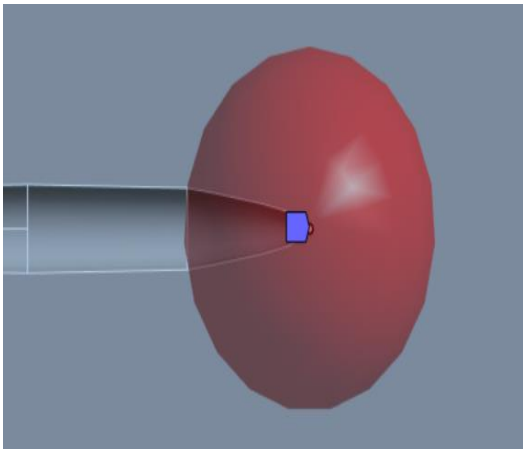

Figure 9: Vertex Sizing

Details of "Vertex Sizing 2" - Sizing	
Scope	
Scoping Method	Geometry Selection
Geometry	1 Vertex
Definition	
Suppressed	No
Type	Sphere of Influence
Sphere Radius	1,35 m
Element Size	0,1 m

Figure 10: Vertex Sizing Details

Mesh Quality Metrics

Element Quality

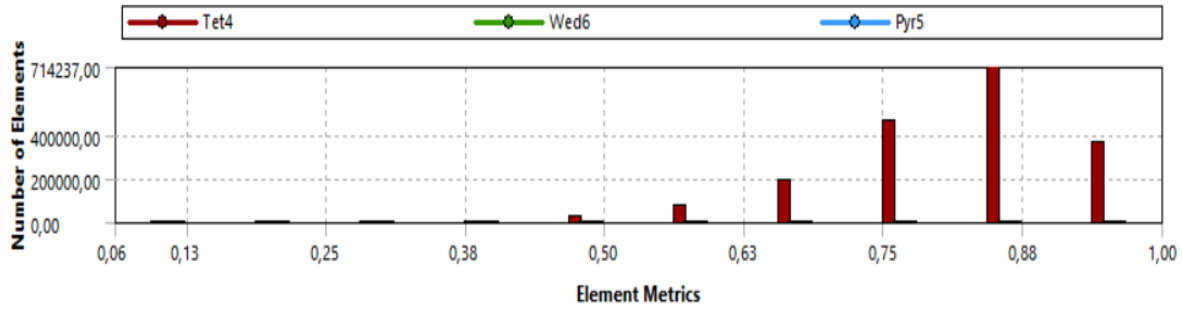

Figure 11: Element Quality Metrics

Aspect Ratio

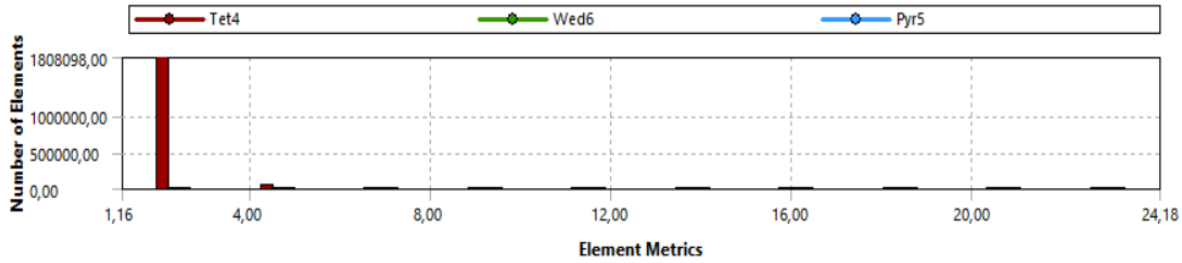

Figure 12: Aspect Ratio Metrics

Skewness

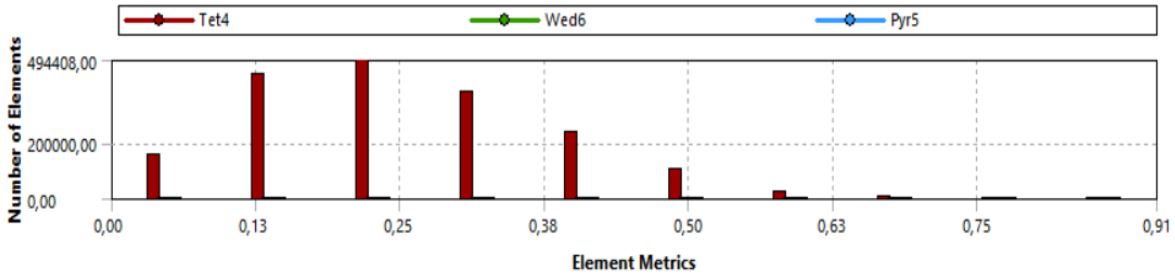

Figure 13: Skewness Metrics

Orthogonal Quality

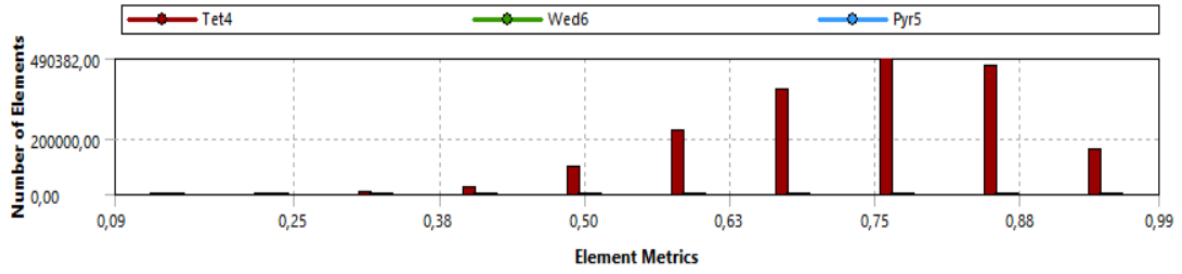

Figure 14: Orthogonal Quality Metrics

Quality Criterion	Warning (Target) Limit	Error (Failure) Limit	Worst
Min Element Quality	Default (0,05)	Default (5e-04)	0,06
Max Aspect Ratio	Default (5)	Default (1000)	24,18
Min Orthogonal Quality	Default (0,05)	Default (5e-03)	0,095
Max Skewness	**Default (0,9)**	Default (0,999)	0,905
Min Tet Collapse	Default (0,1)	Default (1e-03)	0,129

Figure 15: General Mesh Metrics

Named Selections

In this section, one of the important steps necessary for realistically simulating the system under analysis is to describe what the geometry is to the computer to mesh and place the mesh and physics details properly in the Fluent software's analysis. We need to explain what geometry is to specify wall conditions, inlet and outlet conditions, and special conditions we want to define, as well as inflation settings. Fluent has direct counterparts for terms like inlet, outlet, walls, symmetry, and others that we will encounter when setting up the model.

Inlet

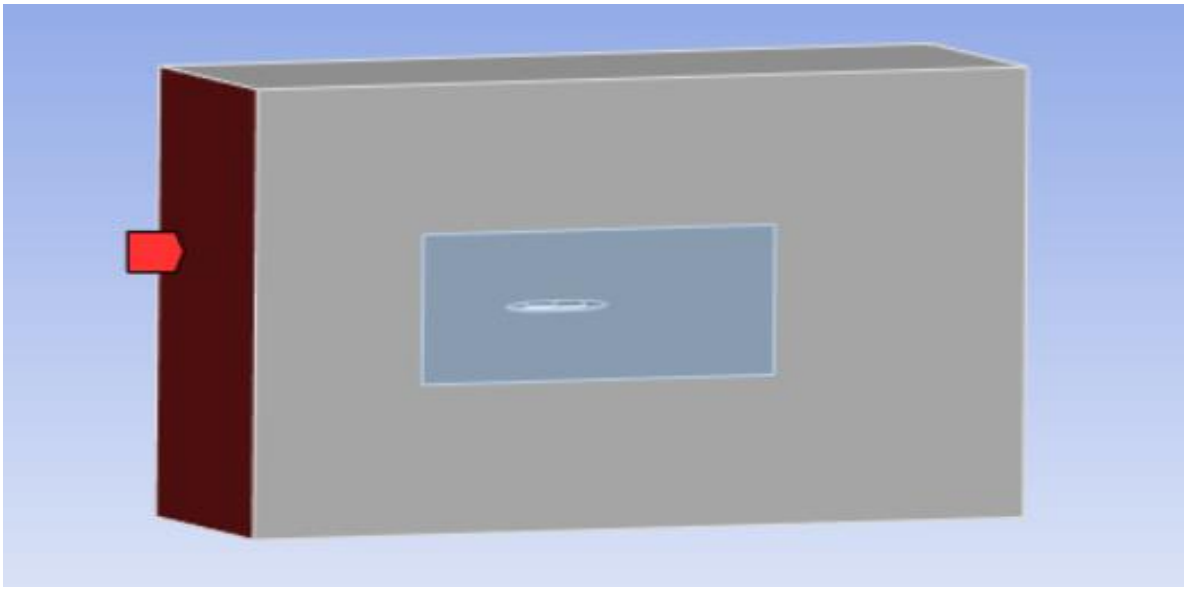

Figure 16: Domain Inlet

Outlet

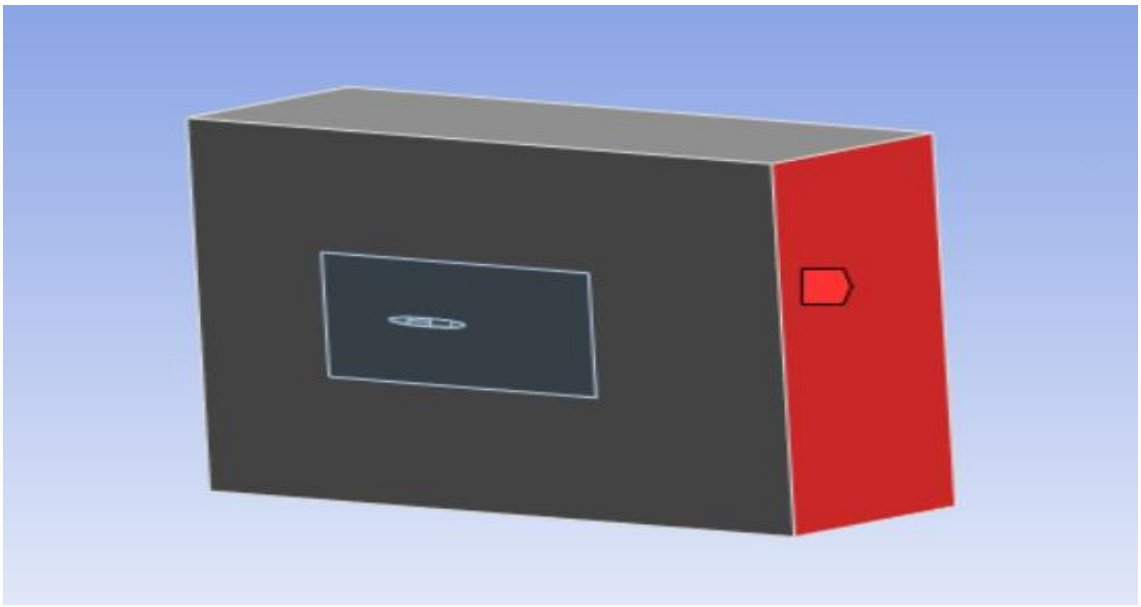

Figure 17: Outlet Domain

Walls

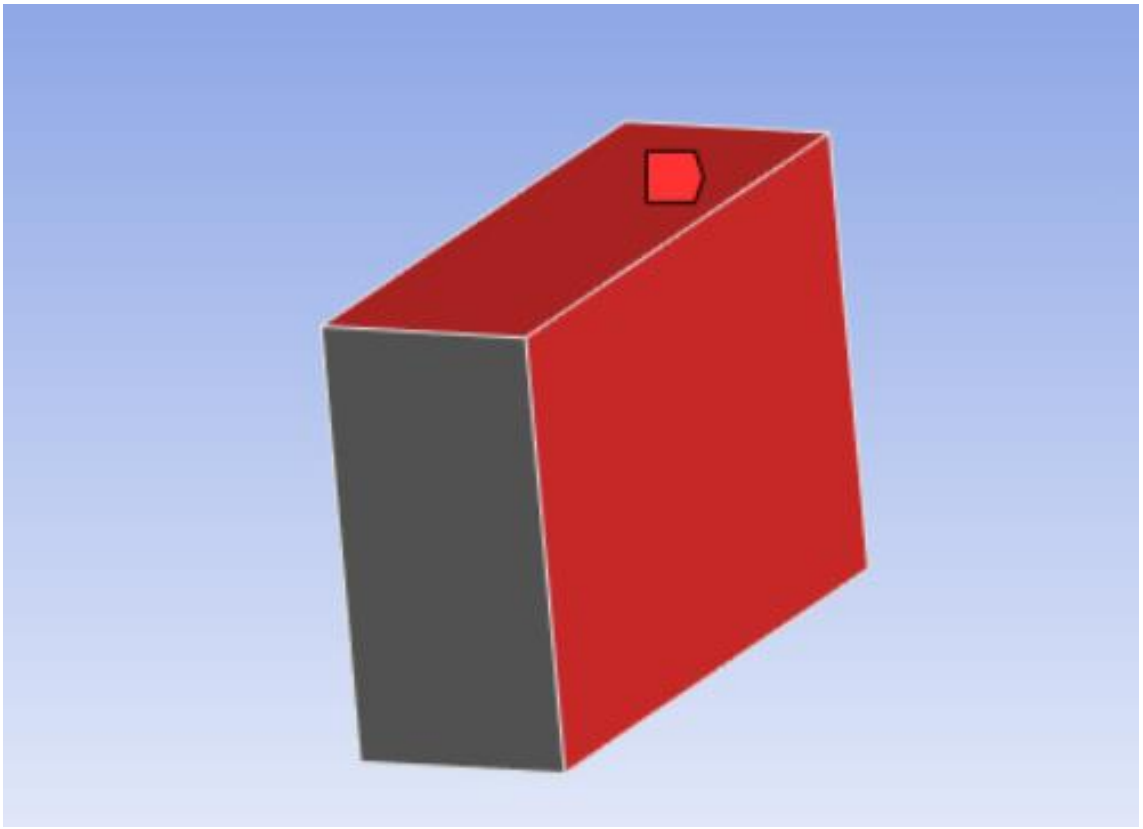

Figure 18: Domain Walls

Fuel Tank and Symmetry

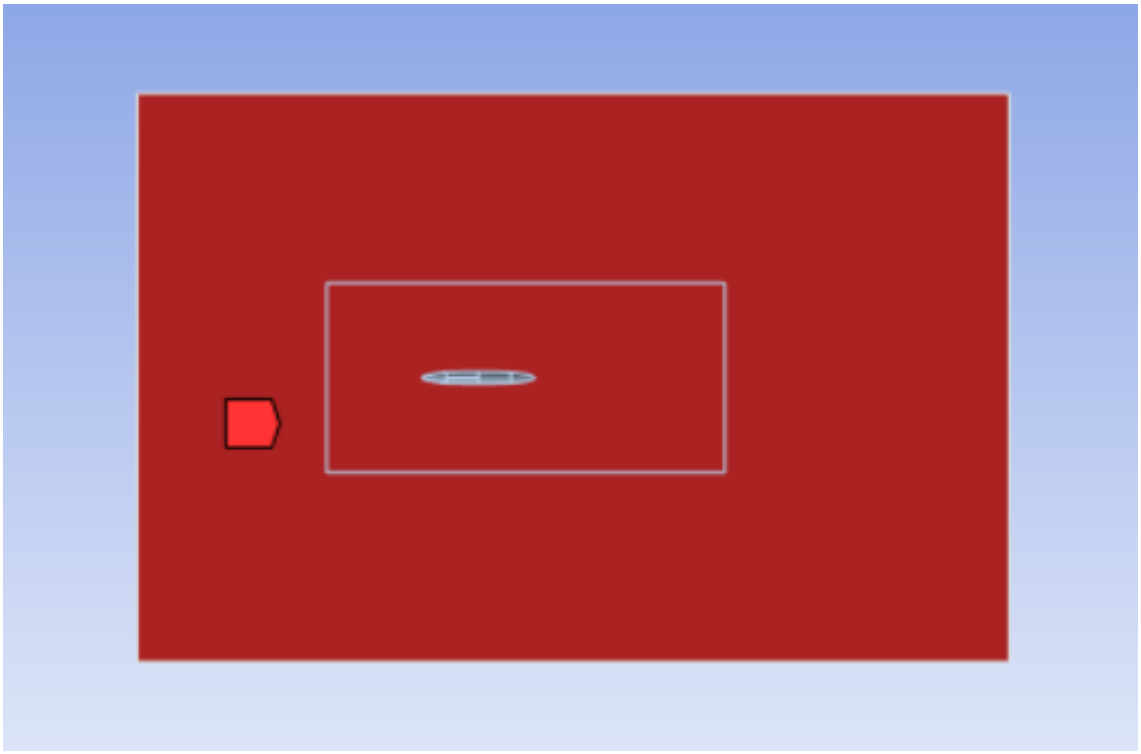

Figure 19: Domain Symmetry

Models and Setup

In this section, we will provide details about the preparation of ambient conditions for our model. We will cover solver type, working fluids, inlet, outlet, and wall conditions. Subsequently, we will discuss solution methods and show the reference area value for the drag coefficient. In this section, we will examine the pre-solution stages.

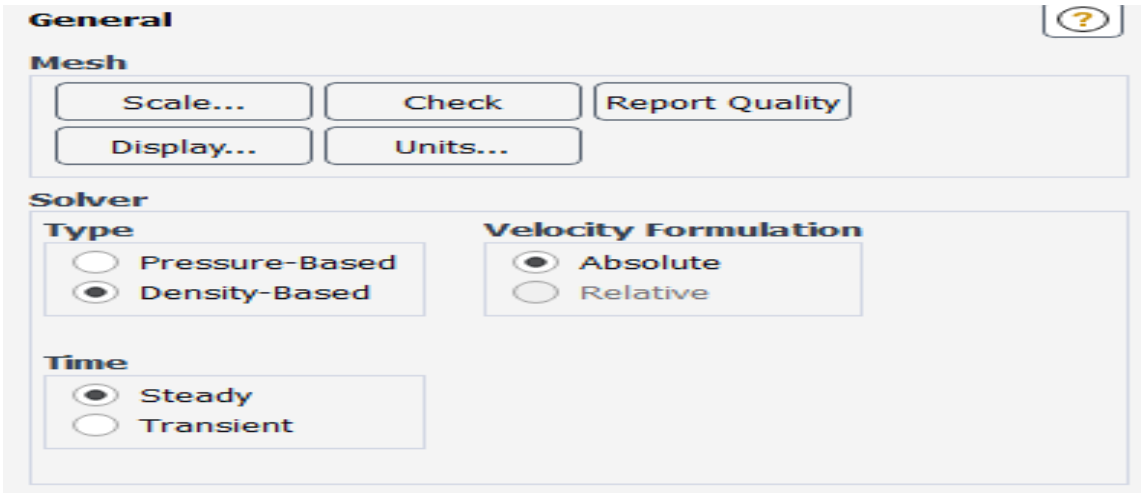

Figure 20: Solver Type

Viscous Model

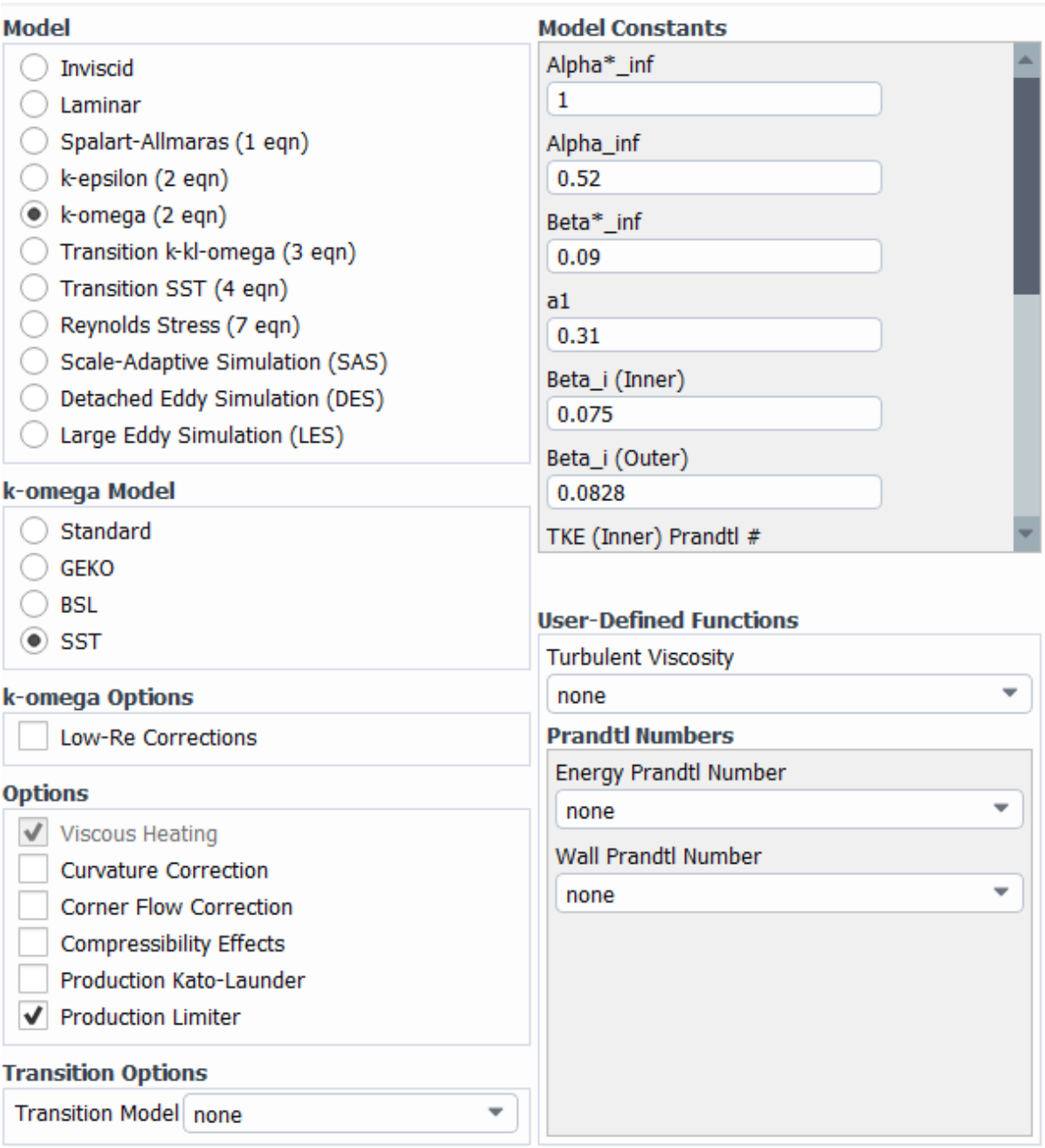

Figure 21: Turbulence Model

Material

While the working fluid in our workflow is air, we choose to assume ideal air for our calculations. Ideal gas behavior is simple and easily calculable, providing a clear mathematical model for supersonic flow analysis. The assumption of ideal gas behavior simplifies the relationship between pressure, temperature, and density, making it an ideal model for analytical calculations in supersonic flows. Ideal gas law calculations are often less complex, facilitating practical and rapid solutions in supersonic flow analyses. The ideal gas models are commonly used for fundamental comparisons and establishing initial parameters in supersonic flow analyses, reducing complexity, and focusing on core concepts.

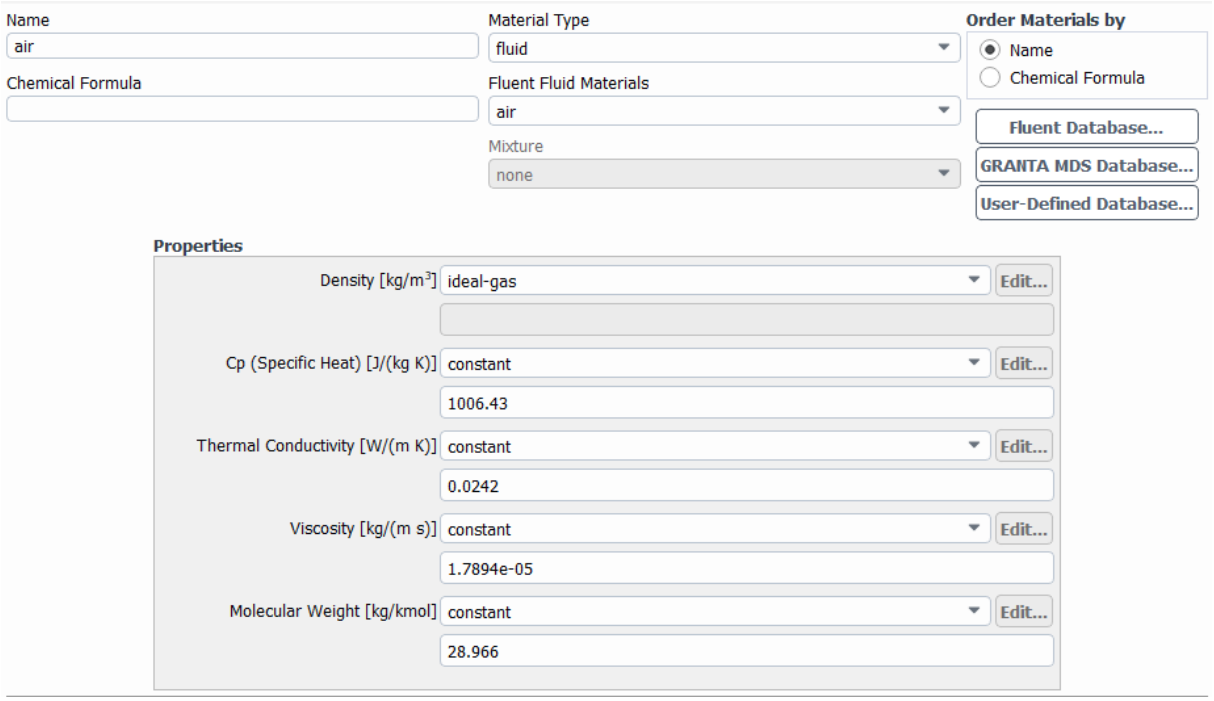

Figure 22: Fluid Properties

Inlet Type

In supersonic flow analyses, the far field inlet is commonly used to initiate the flow from distant regions of the solution domain. The primary reasons for preferring this method include the reduction of interactions, obtaining more accurate results, and ensuring numerical stability.

Air properties at 10000 ft altitude:

1- Absolute pressure (Pa): 7.012x10e4

2- Density (ρ): 0.9093 kg/m^3

3- Dynamic Viscosity(μ): 1.789x10e-5 Ns/m^2

4- Temperature: 268.51 K

We must compute some isentropic relationships to give information to far field inlet, so we used NASA's isentropic relationships calculator.

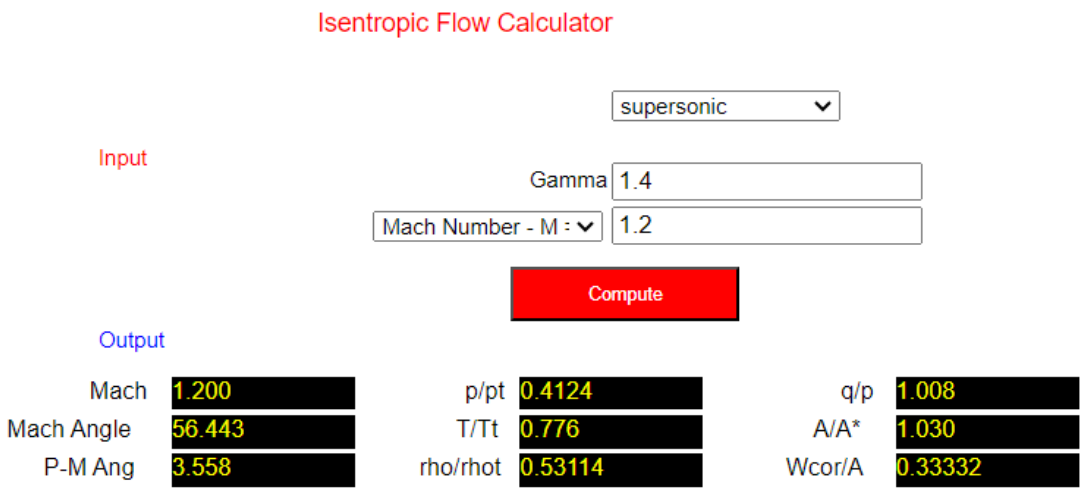

Figure 23: Isentropic Flow Calculator

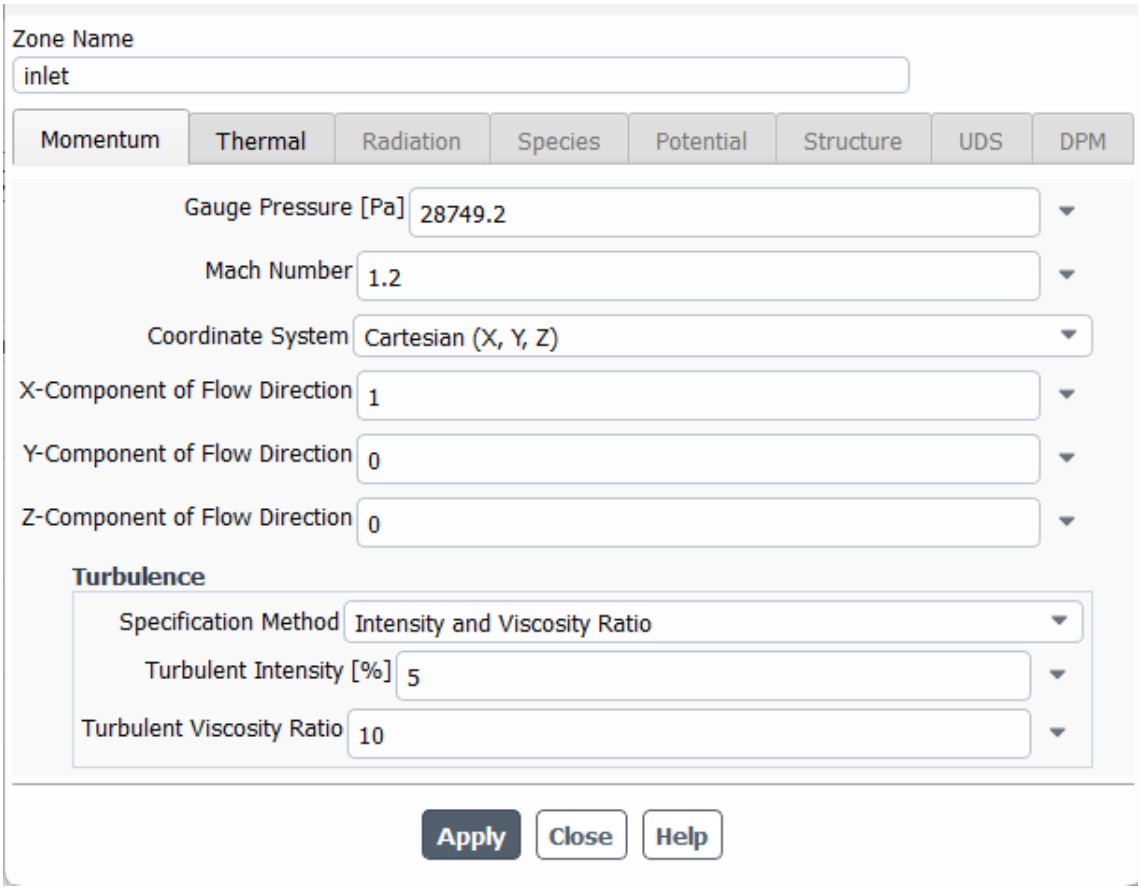

Figure 24: Far Field Inlet Details

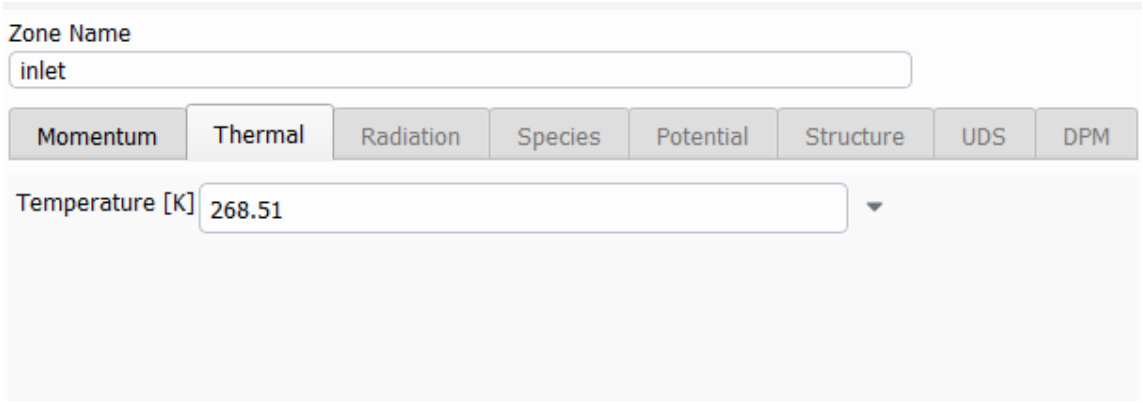

Figure 25: Far Field Temperature Details

Pressure Outlet

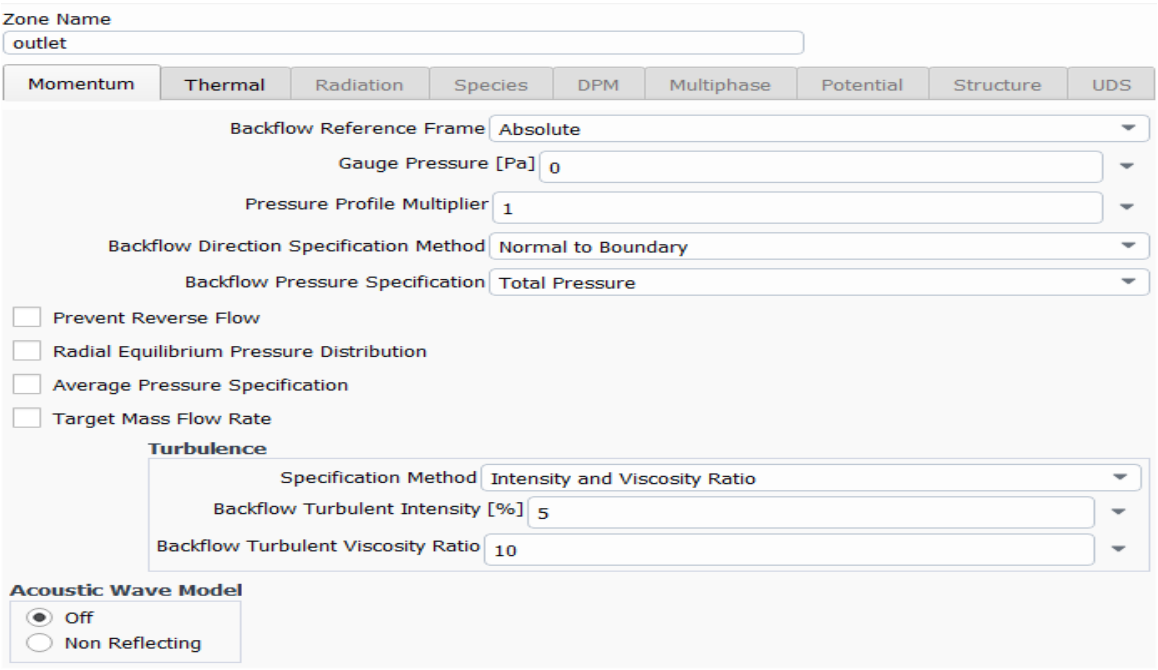

Figure 26: Pressure Outlet Details

Walls

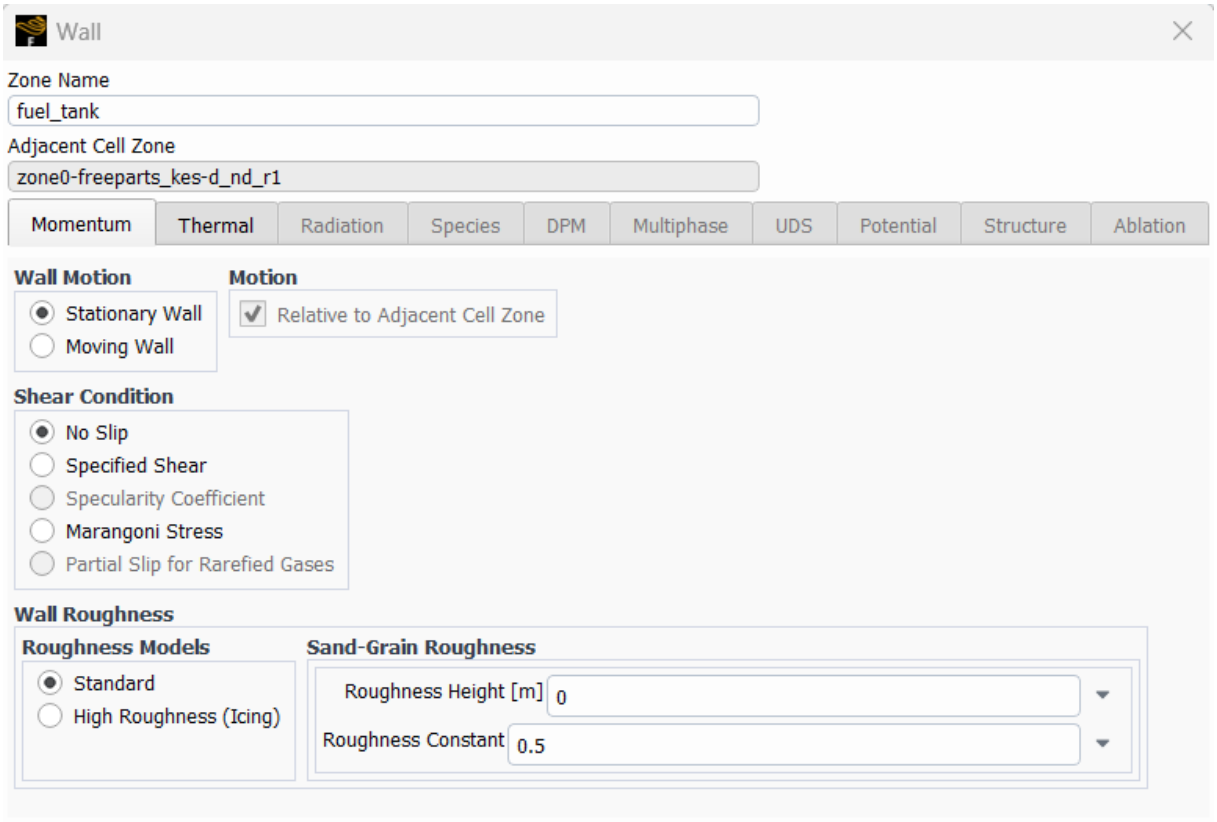

Figure 27: Wall Conditions

Reference Values

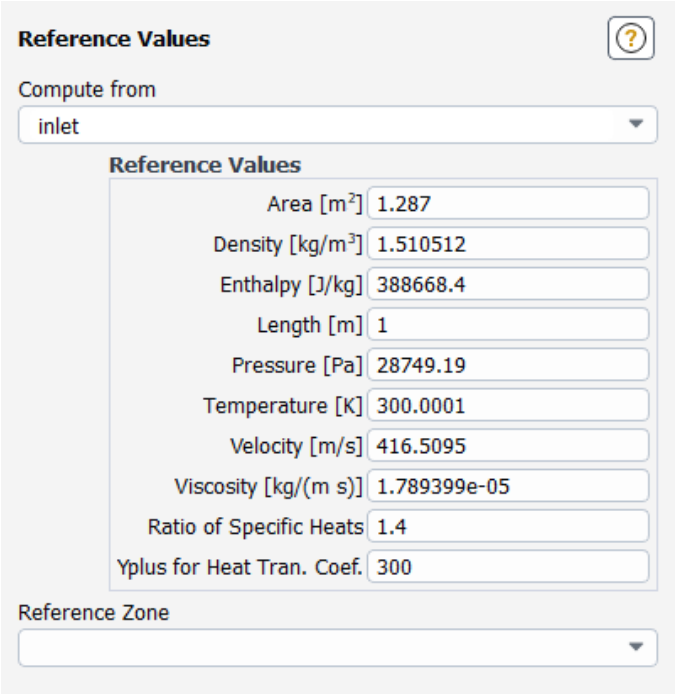

Figure 28: Reference Values

Solution Methods

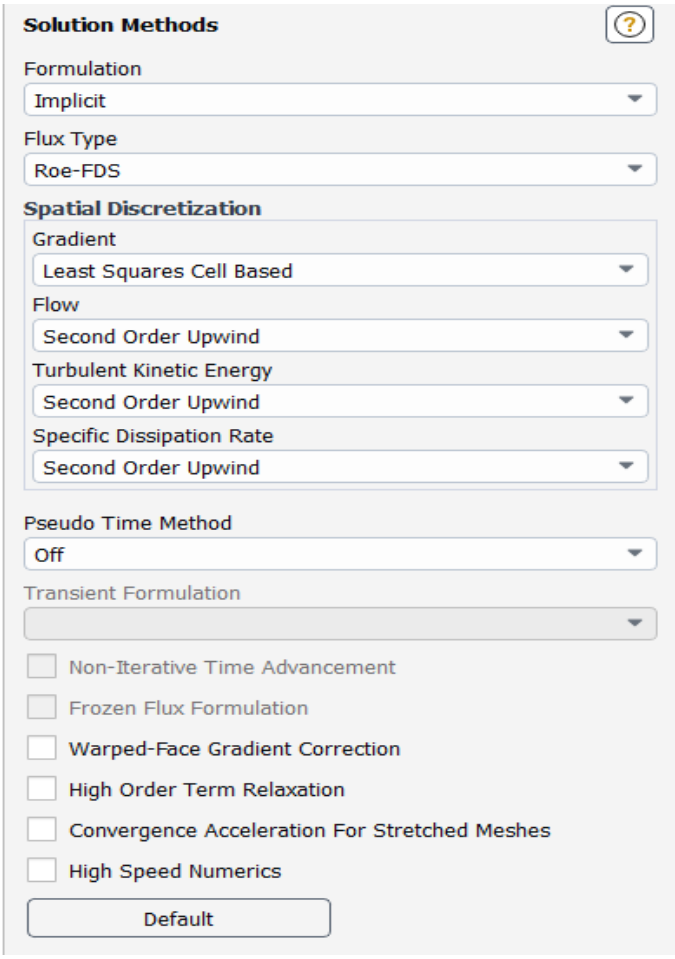

Figure 29: Solution Algorithm

Results

In this section, following the analysis of our first fuel tank, we made design choices for different nose geometries to reduce the drag coefficient. We experimented with Power Series and Von Karman (HAACK Series) nose designs. Von Karman had a very sharp geometry, which resulted in carrying less fuel, so most of the analyses were conducted using the Power Series. Although there were no officially approved data for tank selections by authorities, tanks for aircraft like the F-22, which is approximately 6 meters in length, and for aircraft like the F-16, which is around 4 meters in length, were considered when designing the tanks. These design criteria were considered during the tank design process.

Power Series 0.5 - 1.2L Tank Results (6m Tank)

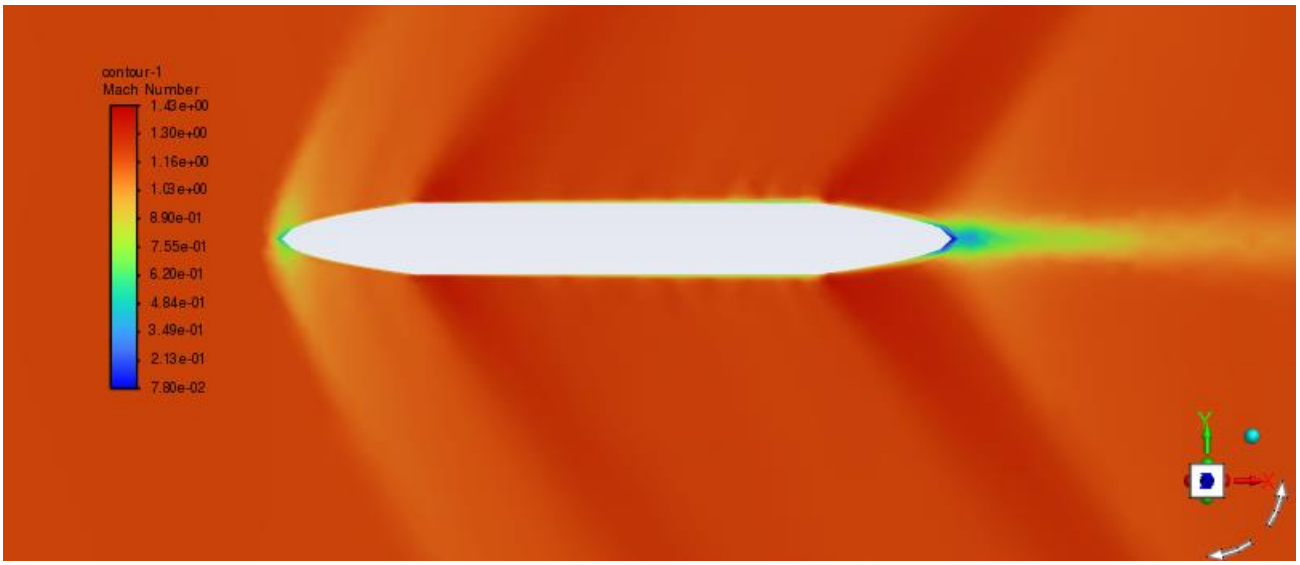

Figure 30: Mach Number Contour

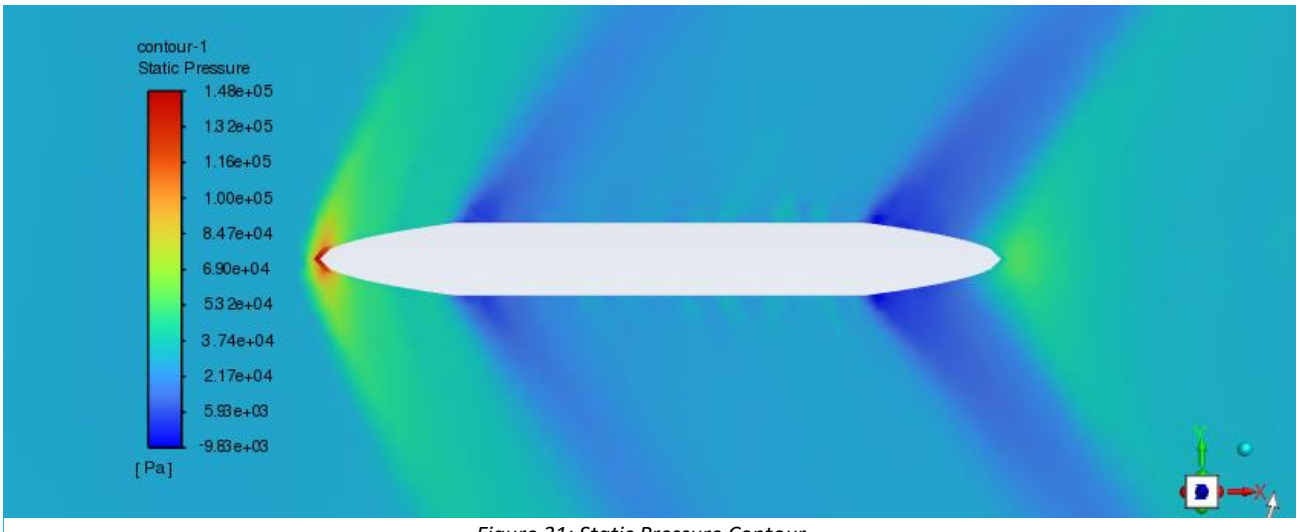

Figure 31: Static Pressure Contour

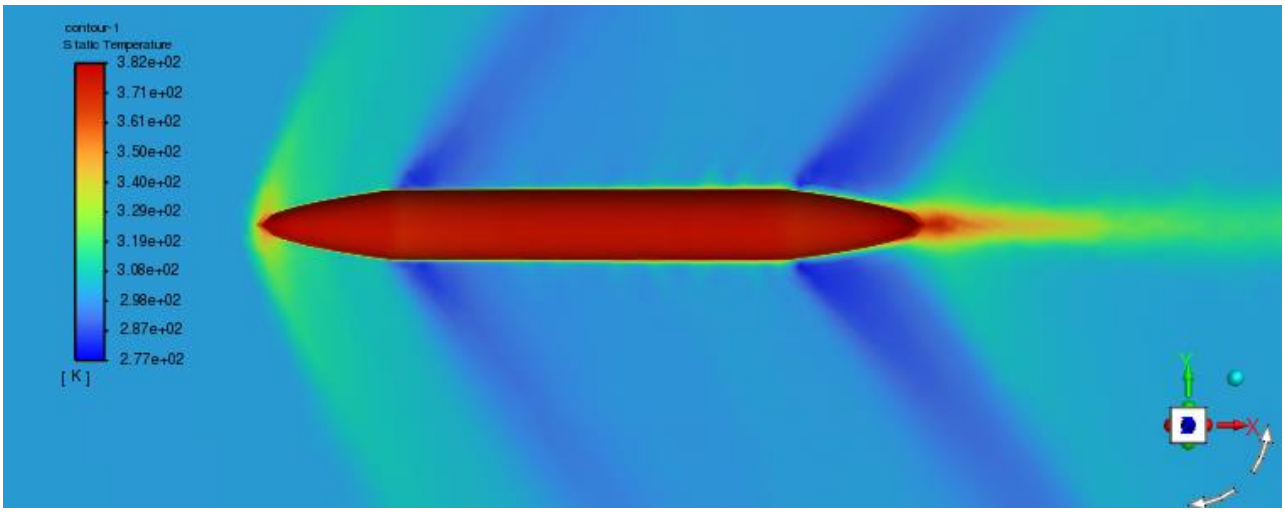

Figure 32: Static Temperature Contour

Forces - Direction Vector (1 0 0)

	Forces [N]			Coefficients		
Zone	Pressure	Viscous	Total	Pressure	Viscous	Total
fuel_tank	7393.4771	1096.5001	8489.9772	0.043845647	0.006502591	0.050348238
Net	7393.4771	1096.5001	8489.9772	0.043845647	0.006502591	0.050348238

Figure 33: Force Report

The coefficient of pressure represents our drag coefficient. This report is generated when you select the force report and name the selection as "fuel tank." The geometry of this tank exhibits a good drag coefficient, like that of a streamlined body. This is a significant difference from common external fuel tanks. We have used the same geometry in the tail section, for example, which is not the case for F-16 tanks.

Power Series 0.5 - 1L Tank Results (6m Tank)

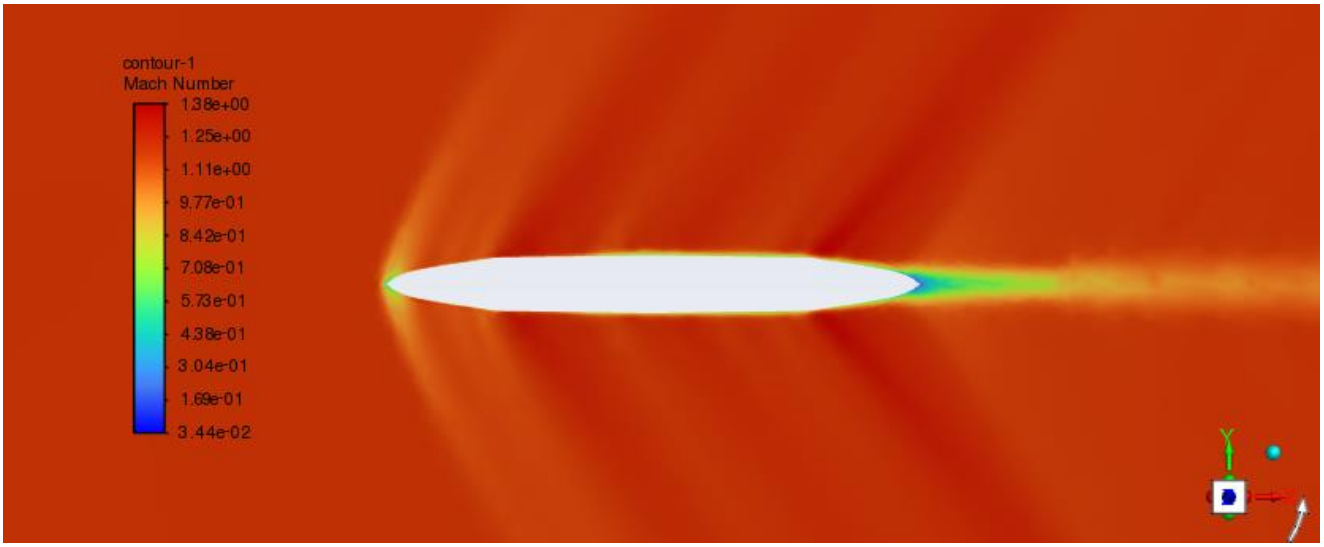

Figure 34: Mach Number Contour

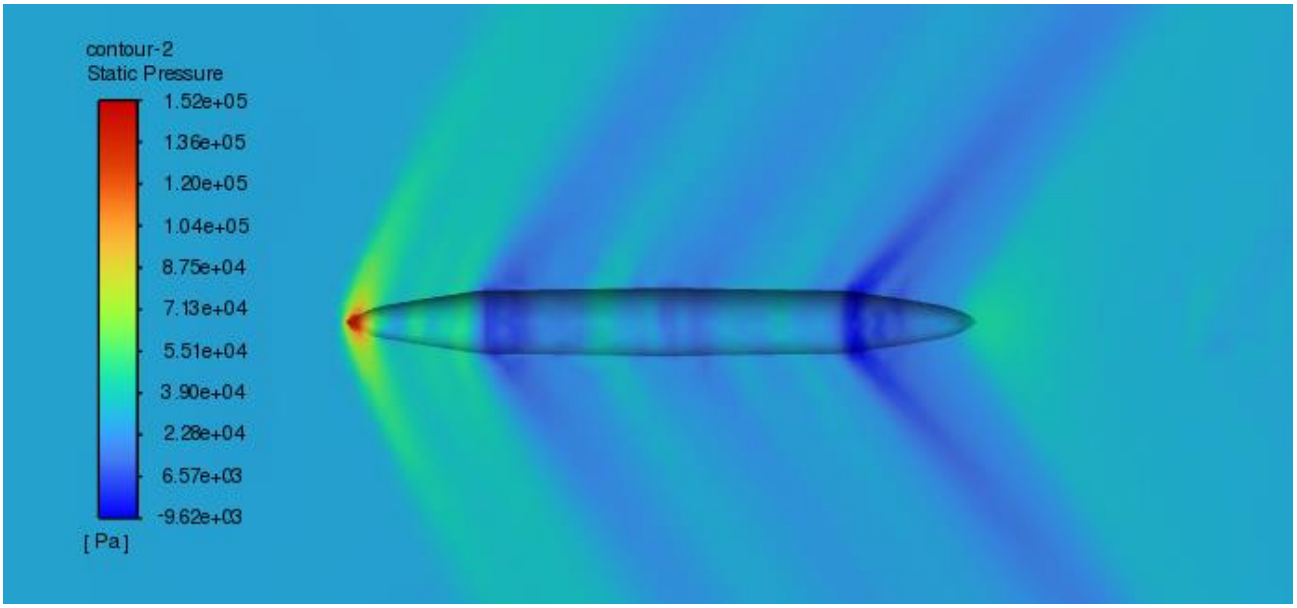

Figure 35: Static Pressure Contour

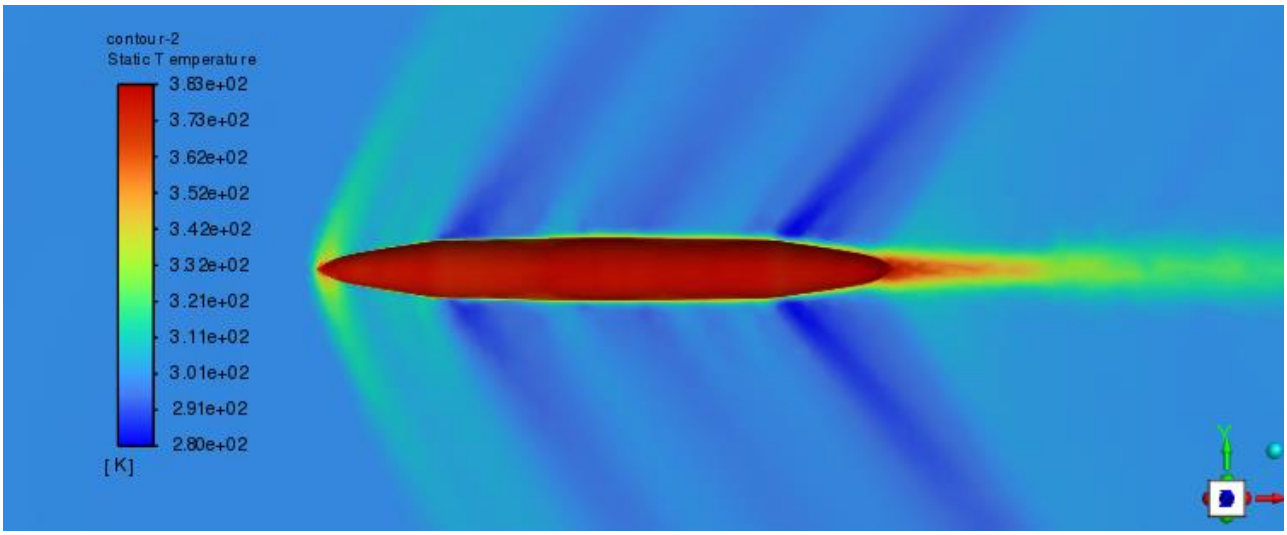

Figure 36: Static Temperature Contour

	Forces [N]			Coefficients		
Zone	Pressure	Viscous	Total	Pressure	Viscous	Total
fuel_tank	7516.2627	835.64117	8351.9039	0.044574026	0.0049556399	0.049529666
Net	7516.2627	835.64117	8351.9039	0.044574026	0.0049556399	0.049529666

Figure 37: Force Report

This tank has good aerodynamic characteristics, and its drag coefficient is nearly the same as the 1.2L geometry.

Power Series 0.5 - 0.75L Tank Results (6m Tank)

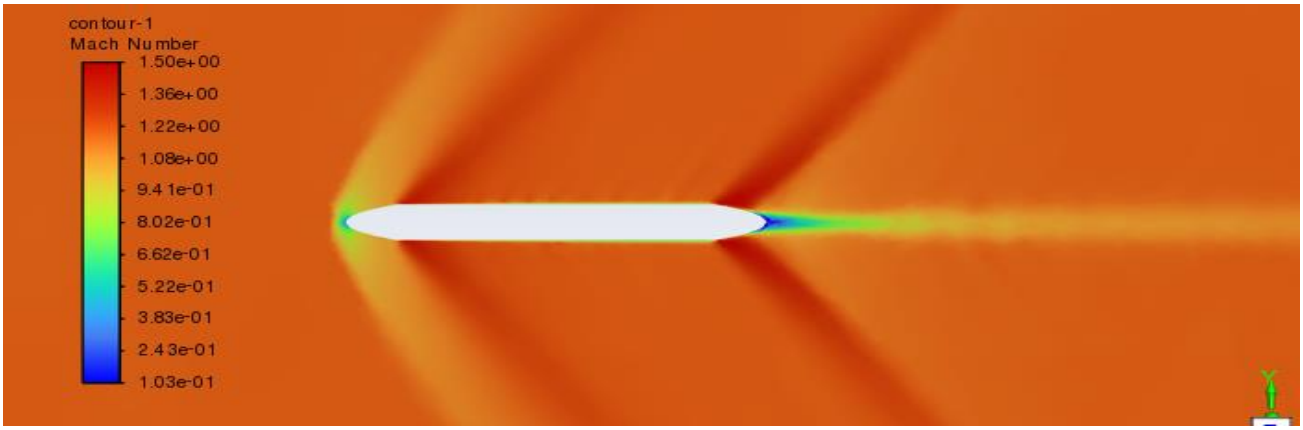

Figure 38: Mach Number Contour

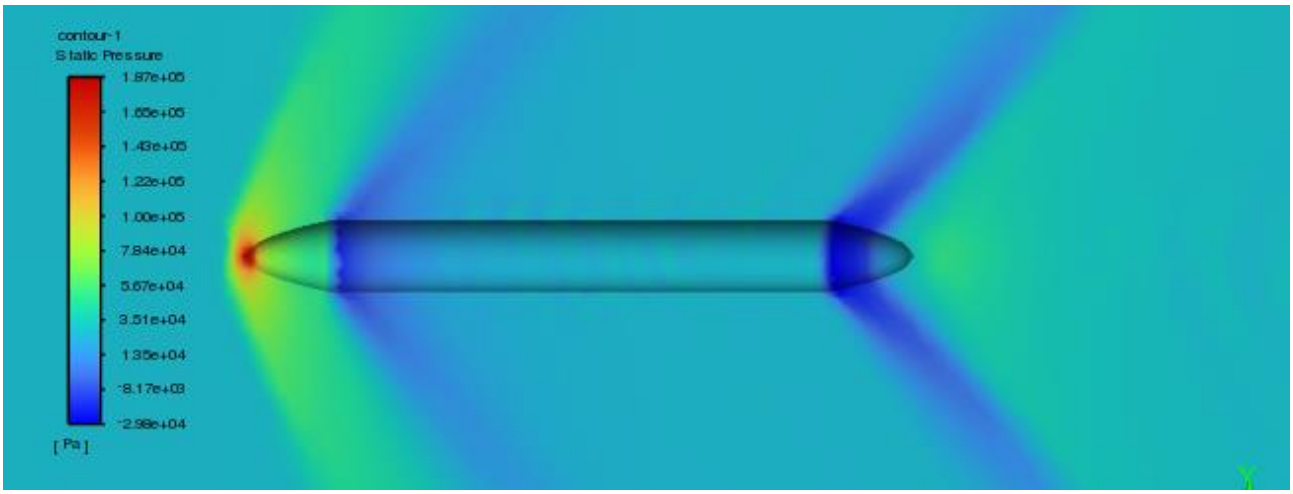

Figure 39: Static Pressure Contour

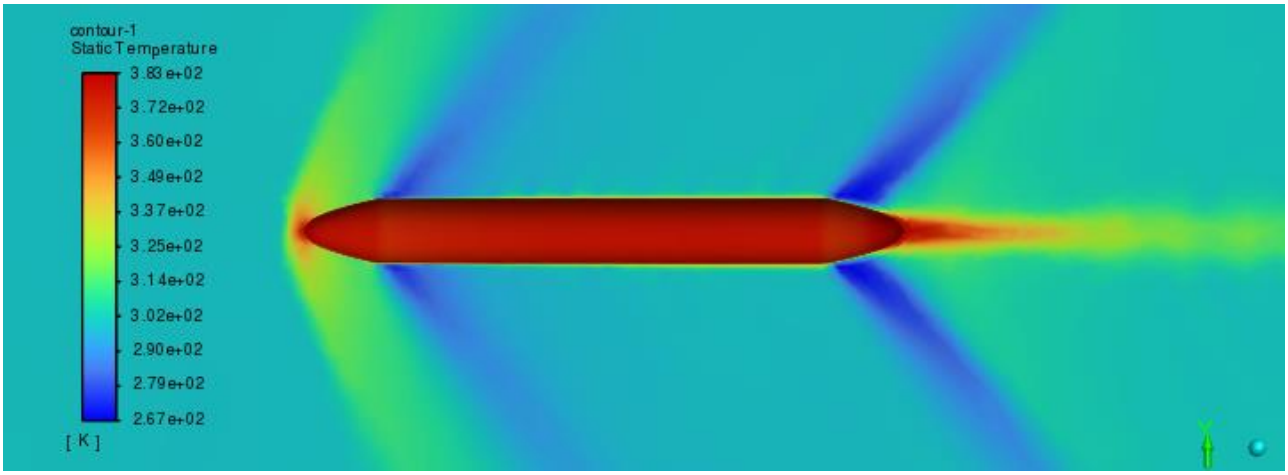

Figure 40: Static Temperature Contour

Forces - Direction Vector (1 0 0)

	Forces [N]			Coefficients		
Zone	Pressure	Viscous	Total	Pressure	Viscous	Total
fuel_tank	12038.722	1116.4432	13155.165	0.071393355	0.0066208548	0.07801421
Net	12038.722	1116.4432	13155.165	0.071393355	0.0066208548	0.07801421

Figure 41: Force Report

This time, the results are not as good as the other two Power Series tank geometries. Unlike them, in this case, the nose length is short, so we can say that when the nose length becomes shorter, the drag coefficient increases.

Power Series 0.5 - 1L Tank Results (4m Tank)

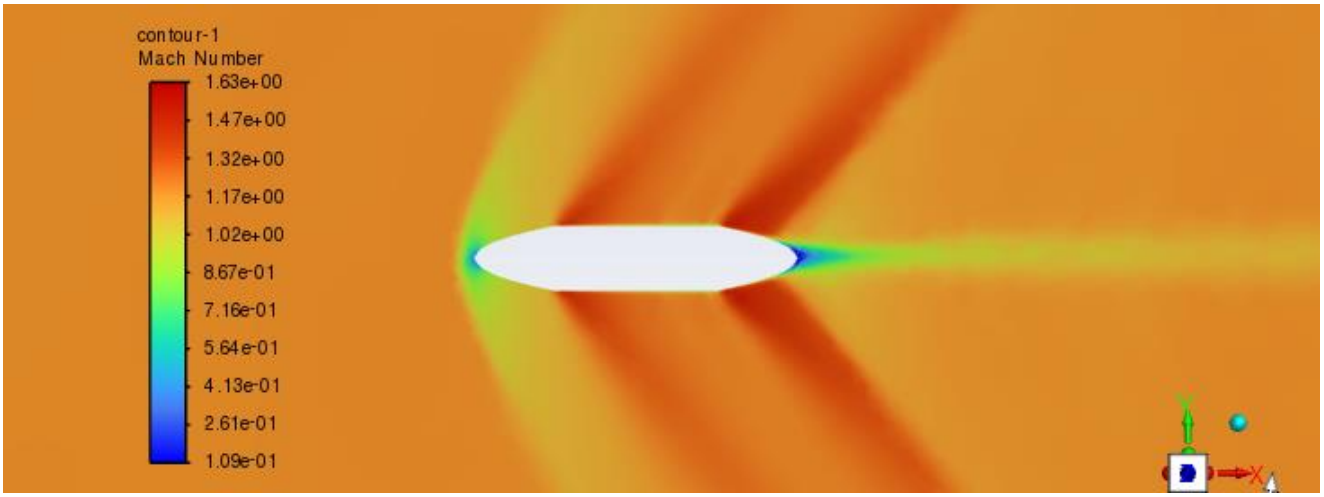

Figure 42: Mach Number Contour

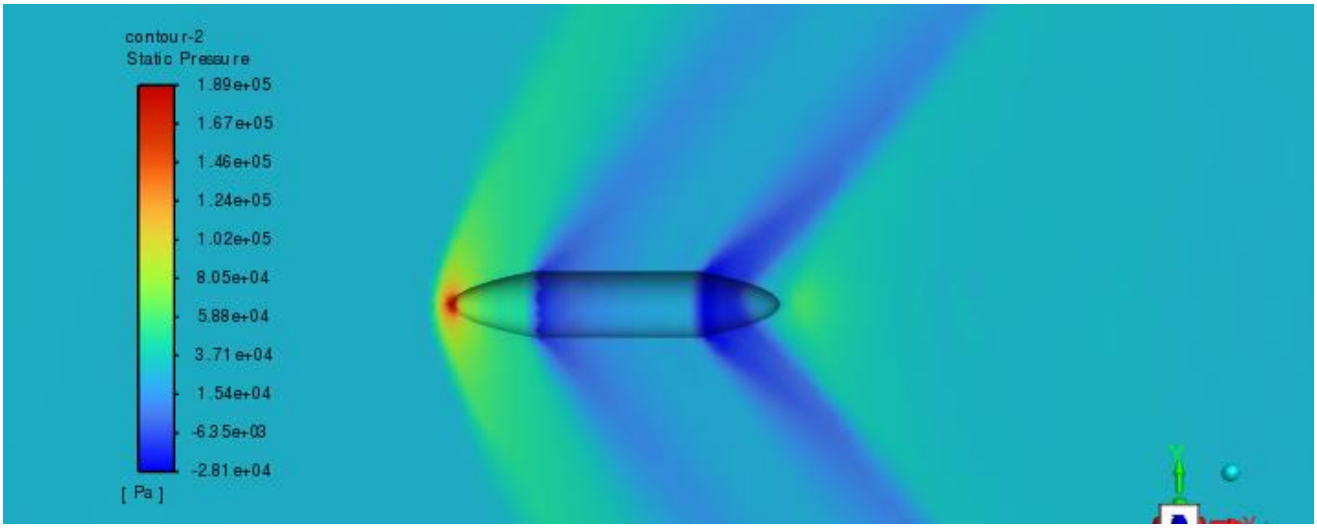

Figure 43: Static Pressure Contour

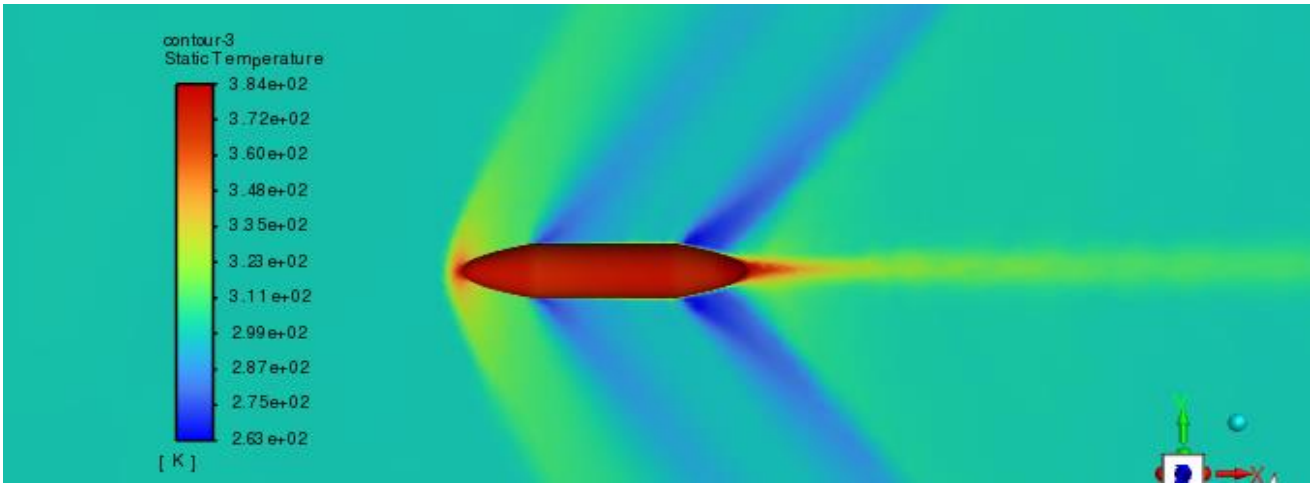

Figure 44: Static Temperature Contour

Forces - Direction Vector (1 0 0)

	Forces [N]			Coefficients		
Zone	Pressure	Viscous	Total	Pressure	Viscous	Total
fuel_tank	18270.611	964.70911	19235.32	0.069376762	0.0036631721	0.073039934
Net	18270.611	964.70911	19235.32	0.069376762	0.0036631721	0.073039934

Figure 45: Force Report

This 4-meter-long, 0.8-meter-diameter fuel tank is better than the previous one, but due to its same nose length and smaller total length, it is not as good as the 6-meter version.

Power Series 0.5 - 0.75 L Fuel Tank Results (4m Tank)

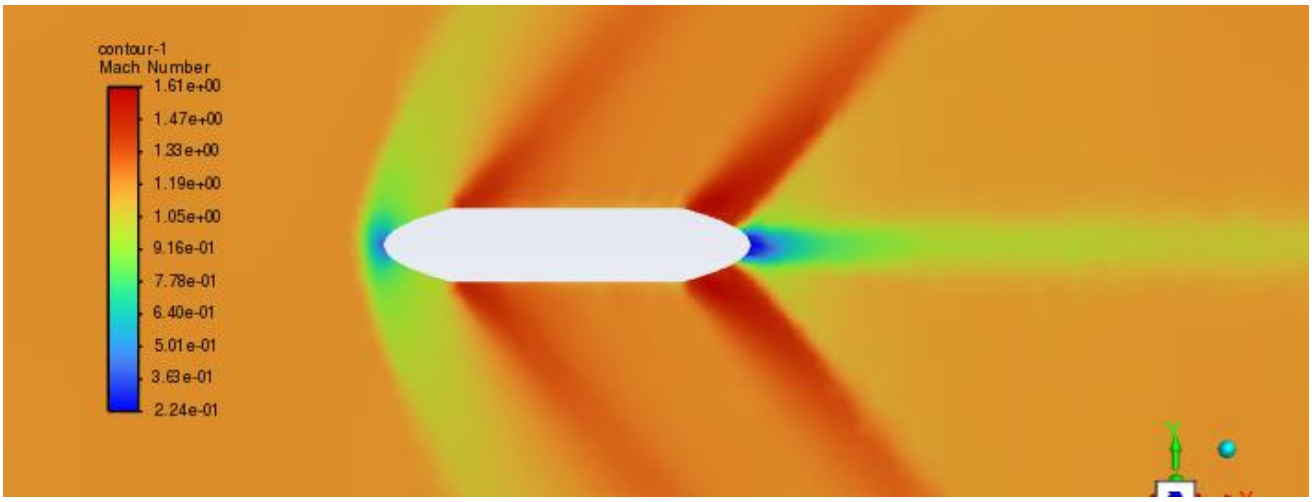

Figure 46: Mach Number Contour

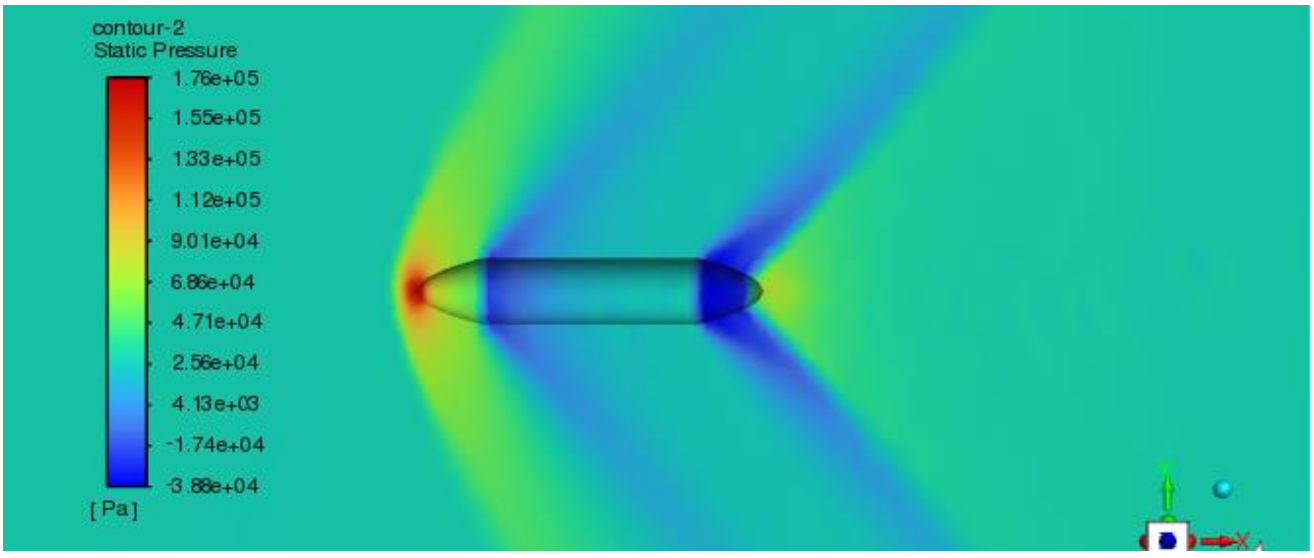

Figure 47: Static Pressure Contour

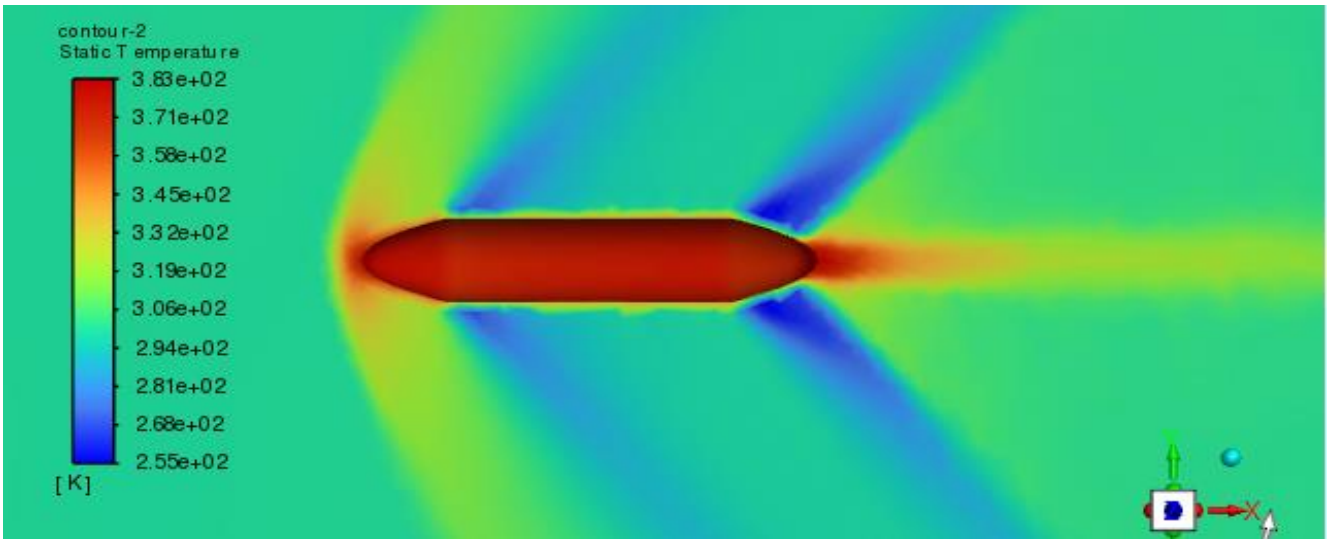

Figure 48: Static Temperature Contour

Forces - Direction Vector (1 0 0)

	Forces [N]			Coefficients		
Zone	Pressure	Viscous	Total	Pressure	Viscous	Total
fuel_tank	25436.527	545.0683	25981.596	0.096586785	0.0020697163	0.098656501
Net	25436.527	545.0683	25981.596	0.096586785	0.0020697163	0.098656501

Figure 49: Force Report

So, in this geometry, both the nose length and total length are shorter, and this one has worse drag characteristics. Using our results, we can conclude that slender bodies provide better drag characteristics, as expected.

As we mentioned earlier, our initial preference was the Power Series because the Haack Series has a sharp shape, and we are not designing rockets. If we had similar requirements, our external fuel tanks could be considered as fuselage. However, if the Haack Series can demonstrate extraordinary performance, then perhaps we could opt for the Haack Series. Therefore, we evaluated two geometries in the Haack Series analysis.

Haack Series 1.5L Fuel Tank Results (6m Tank)

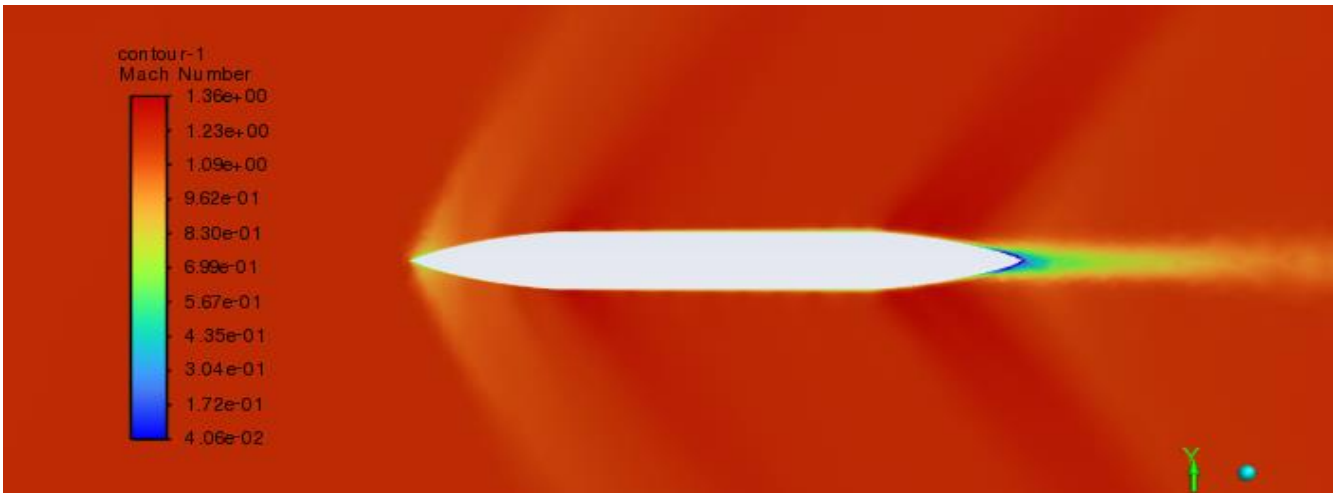

Figure 50: Mach Number Contour

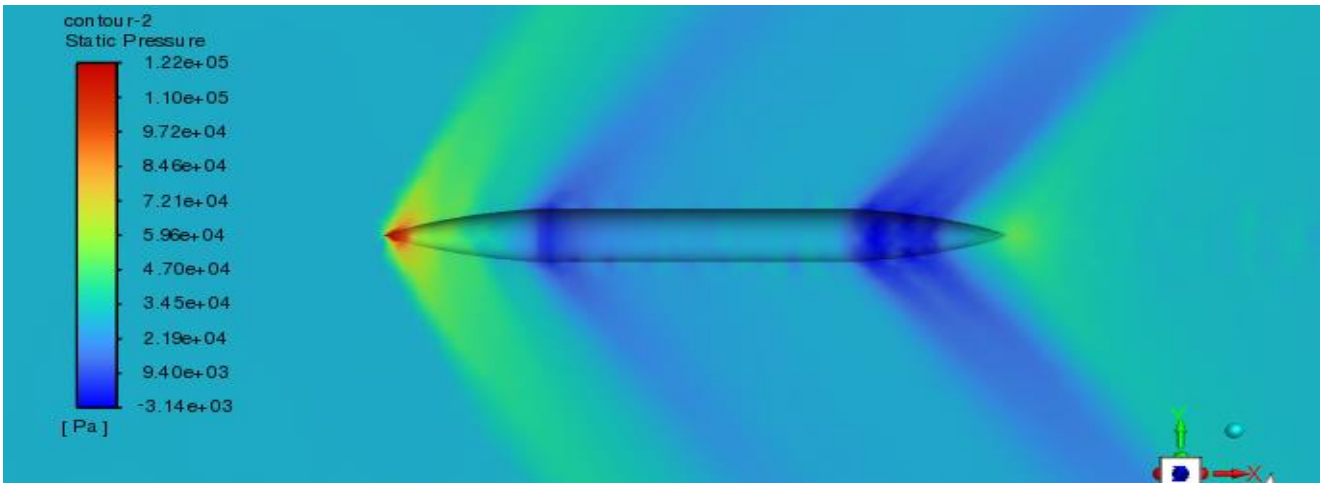

Figure 51: Static Pressure Contour

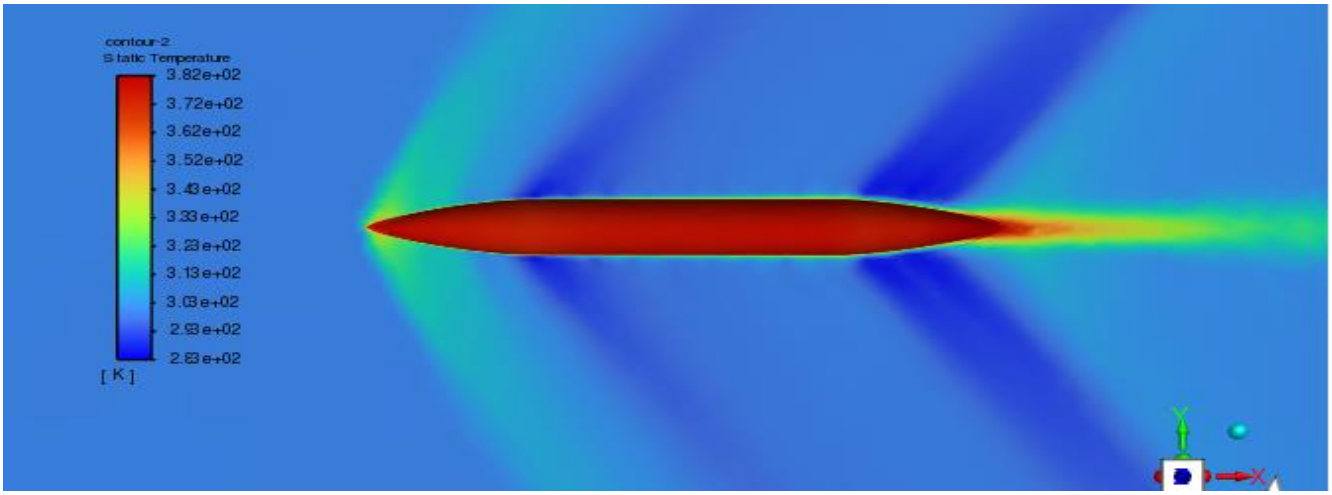

Figure 52: Static Temperature Contour

```
Forces - Direction Vector (1 0 0)
                          Forces [N]                                    Coefficients
Zone                      Pressure        Viscous         Total         Pressure        Viscous         Total
fuel_tank                 6805.8604       940.89545       7746.7558     0.040360973     0.0055798171    0.04594079
------------------------- --------------- --------------- ------------- --------------- --------------- ---------------
Net                       6805.8604       940.89545       7746.7558     0.040360973     0.0055798171    0.04594079
```

Figure 53: Force Report

Haack Series 1L Fuel Tank Results (6m Tank)

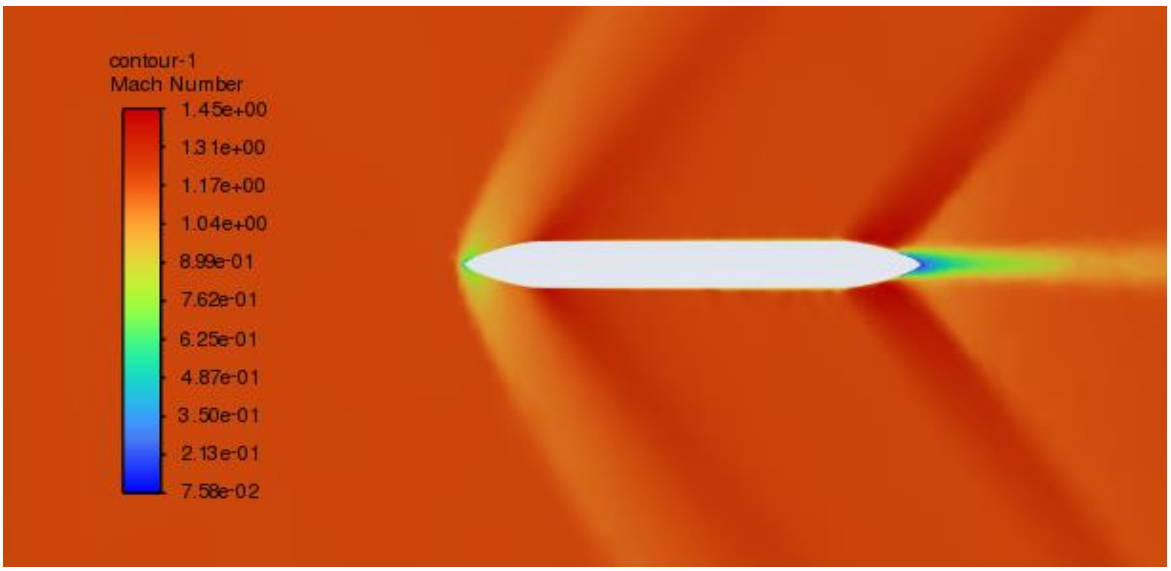

Figure 54: Mach Number Contour

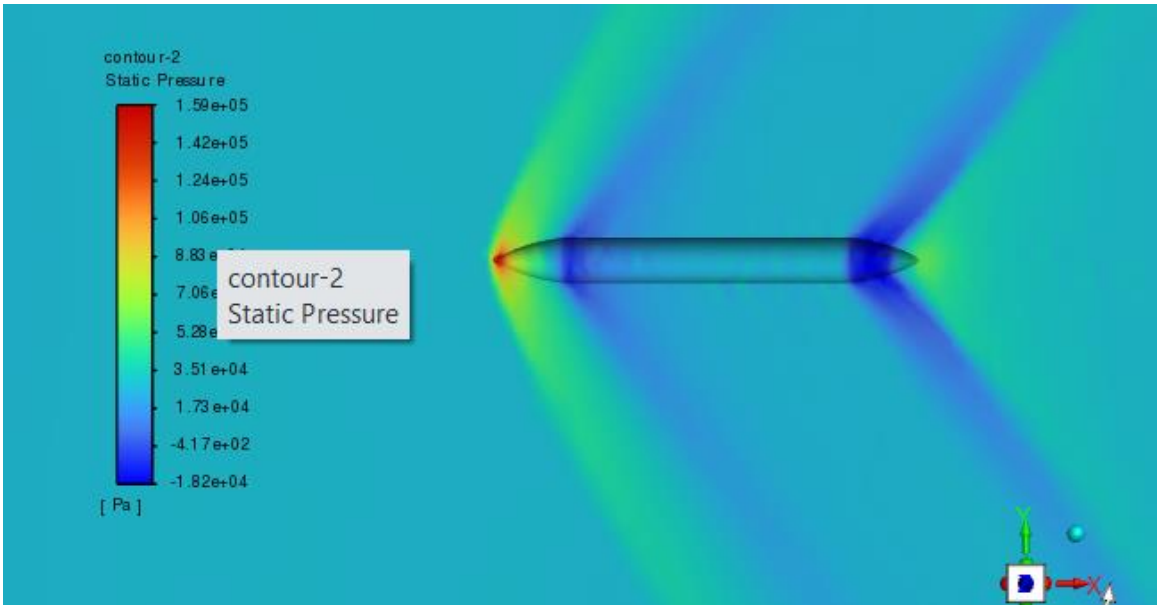

Figure 55: Static Pressure Contour

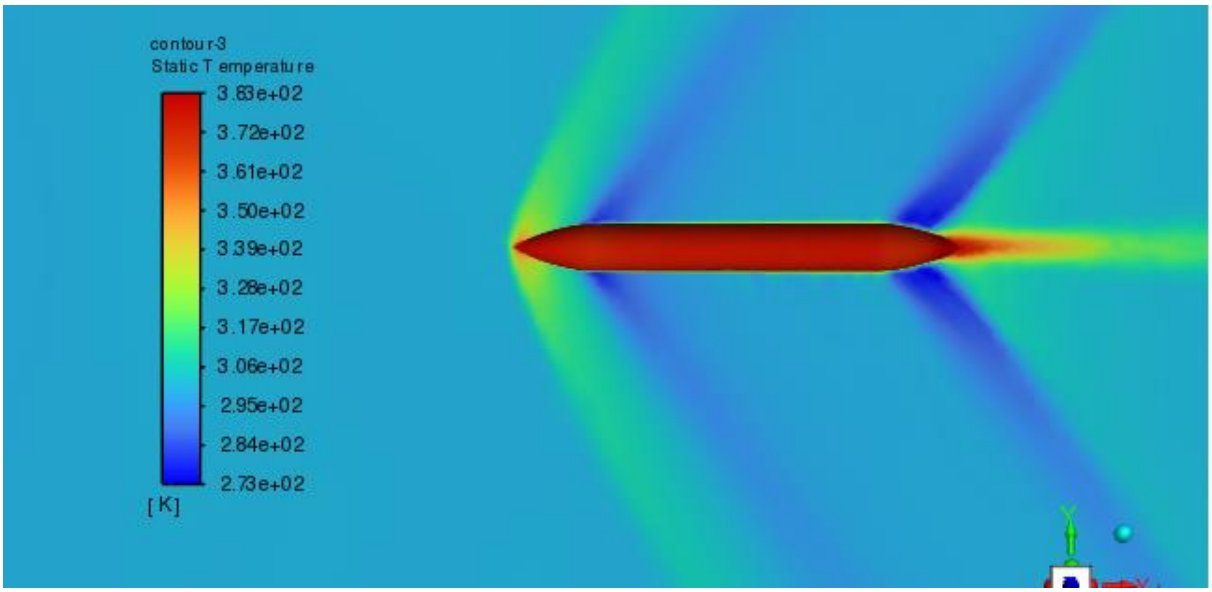

Figure 56: Static Temperature Contour

Forces - Direction Vector (1 0 0)

	Forces [N]			Coefficients		
Zone	Pressure	Viscous	Total	Pressure	Viscous	Total
fuel_tank	10110.352	1110.1521	11220.504	0.059957517	0.0065835459	0.066541063
Net	10110.352	1110.1521	11220.504	0.059957517	0.0065835459	0.066541063

Figure 67: Force Report

The analyses of the Haack series produced results that were approximately similar to those of the Power series analyses. The fuel tank, named HAACK series 1L, yielded results around 0.06, while the Power series geometries in a similar range provided better results. The most favorable outcome was achieved with HAACK series 1.5L, which exhibited results close to those of the Power series and had a geometry resembling a bullet. Due to these reasons, the decision was made to proceed with the Power series.

Tank Geometries Comparison

Tank Name	Drag Coefficient (Cd)
Power Series 1.2 L (6m)	0.0438
Power Series 1L (6m)	0.0445
Power Series 0.75 L (6m)	0.0731
Power Series 1L (4m)	0.0693
Power Series 0.75 L (4m)	0.0965
Haack Series 1L (6m)	0.0599
Haack Series 1.5L (6m)	0.0403

As we can see from the table, the Haack Series exhibits the best performance. However, when considering other aspects, the tank geometry is not suitable for our application due to its volume and shape. The performance of Power Series 0.75L is almost equivalent to the main fuel tank. Other suitable performances come from Power Series 1.2L and 1L. From now on, we will investigate the effect of pylon length on our system.

Pylon Analysis

In our upcoming study, we will conduct calculations for the pylon length, which will involve the wing, pylon, and fuel tank. While using a real fighter jet model in the study could be beneficial, it would require a larger domain, a more extensive mesh network, and longer computation times. Additionally, creating a CAD design would be an extra effort. Although the tank designs adhere to real dimensions, suitable measurements for the aircraft design are not available. Therefore, we have adopted an infinite body approach and made designs in the simplest way that is appropriate for the project's precision.

Throughout the ongoing process, the model details will remain the same, except for the reference values. This is because it is necessary to keep the environmental conditions constant.

Domain and Mesh Data

Pylon and Tank Structure Domain

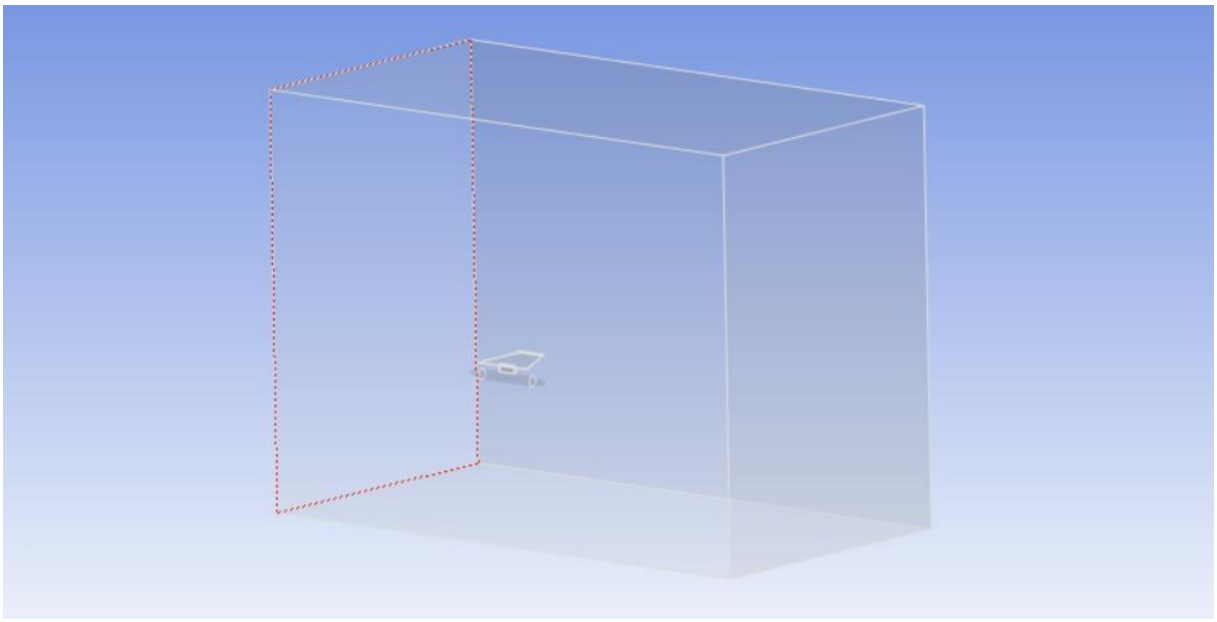

Figure 68: Solution Domain

The area dimensions remained the same, but of course we used a single body and different mesh details in this area.

Mesh Data

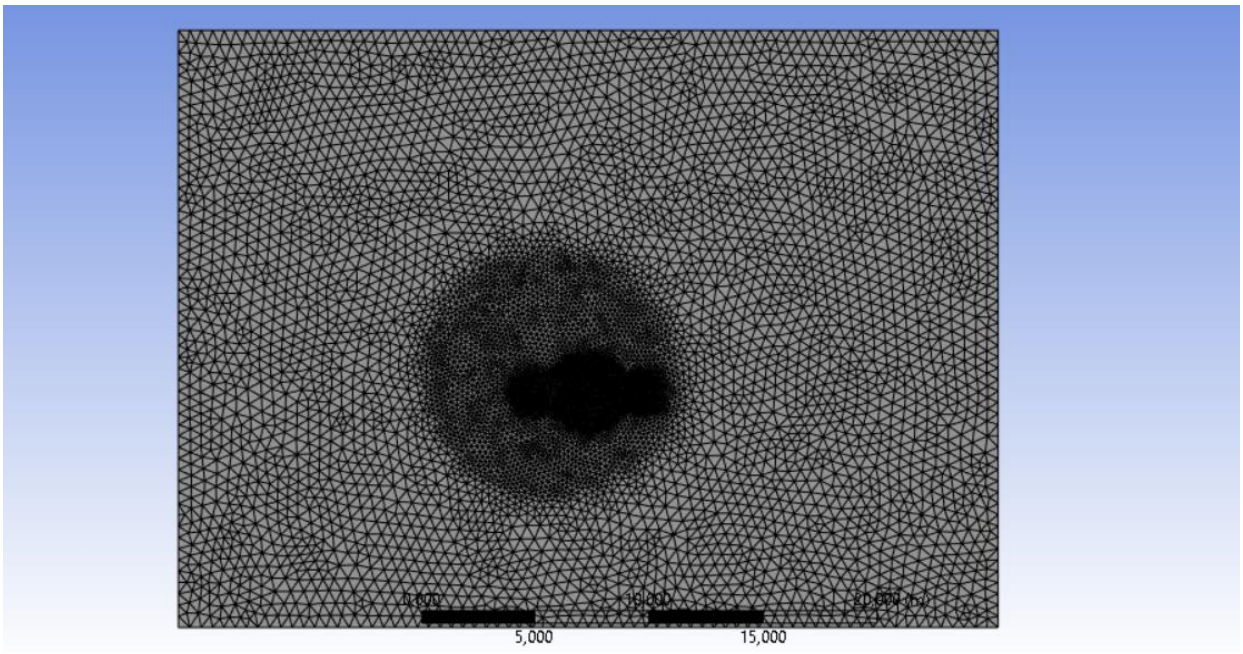

Figure 69: Solution Mesh

Global Mesh Details

Display	
Display Style	Use Geometry Setting
Defaults	
Physics Preference	CFD
Solver Preference	Fluent
Element Order	Linear
Element Size	0,5 m
Export Format	Standard
Export Preview Surface Mesh	No
Sizing	
Use Adaptive Sizing	No
Growth Rate	Default (1,2)
Max Size	Default (1, m)
Mesh Defeaturing	Yes
Defeature Size	Default (2,5e-003 m)
Capture Curvature	Yes
Curvature Min Size	Default (5,e-003 m)
Curvature Normal Angle	Default (18,°)
Capture Proximity	Yes
Proximity Min Size	Default (5,e-003 m)
Proximity Gap Factor	Default (3,)
Proximity Size Sources	Faces and Edges
Bounding Box Diagonal	48,449 m

Figure 70: Global Mesh Details

Local Mesh Details

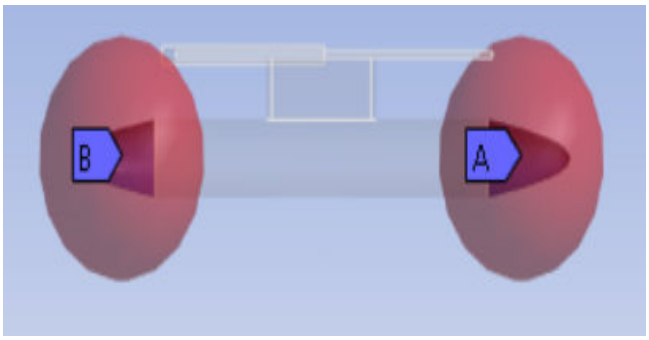

Figure 71: Sphere of Influence Details

Definition	
Suppressed	No
Type	Sphere of Influence
Sphere Center	
Sphere Radius	1, m
Element Size	0,1 m
Control Messages	No

Figure 72: Vertex Sizing

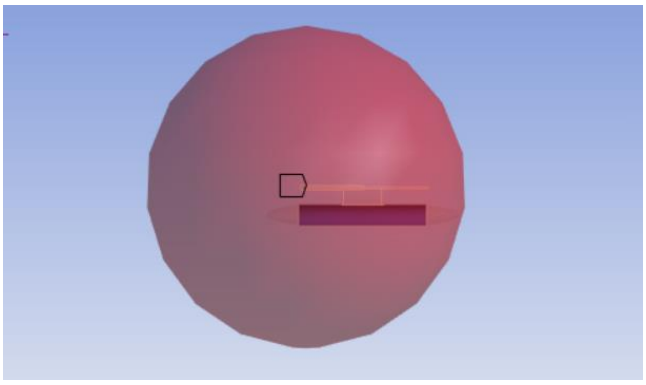

Figure 73: Sphere of Influence Details

Definition	
Suppressed	No
Type	Sphere of Influence
Sphere Center	Global Coordinate System
Sphere Radius	5, m
Element Size	0,2 m
Control Messages	No

Figure 74: Vertex Sizing

Pylon Model and Setup

As mentioned before model so turbulence working fluid wall conditions are same only difference comes from reference values.

Reference Values

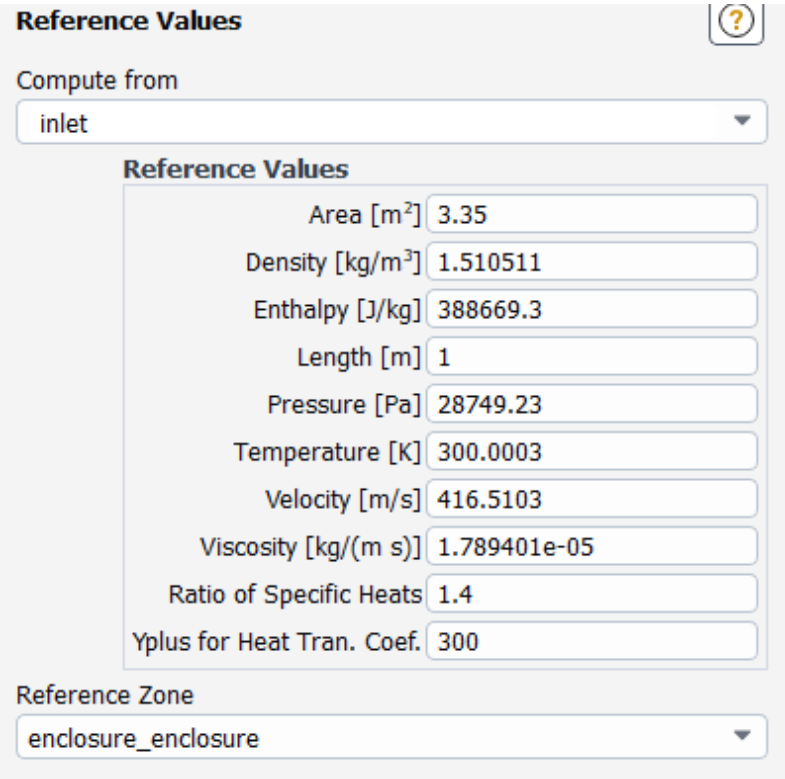

Figure 75: Reference Values

Results (Pylon)

1m Pylon Length Results

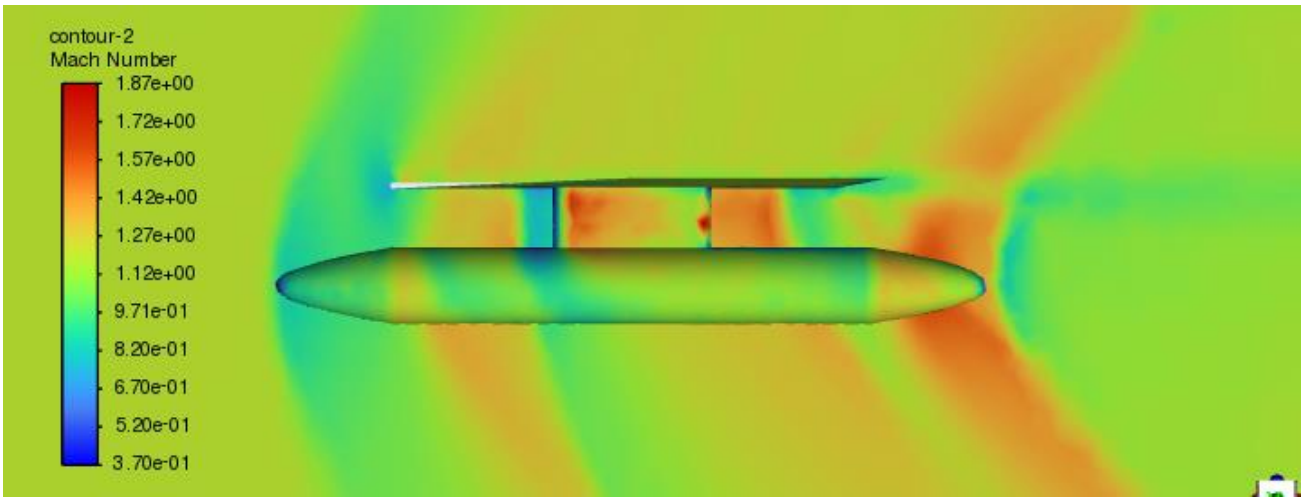

Figure 76: Mach Number Contour

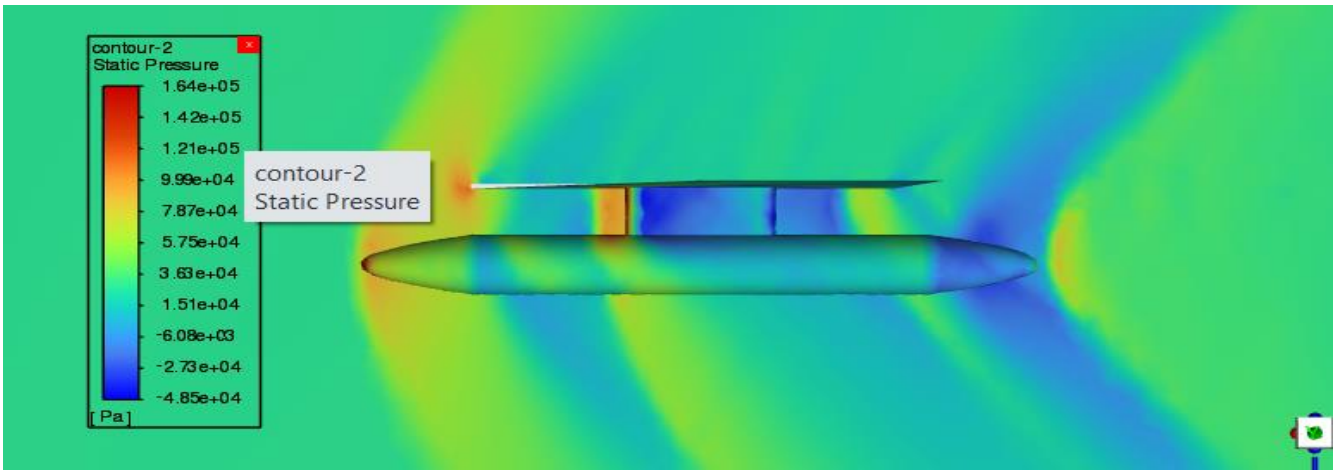

Figure 77: Static Pressure Contour

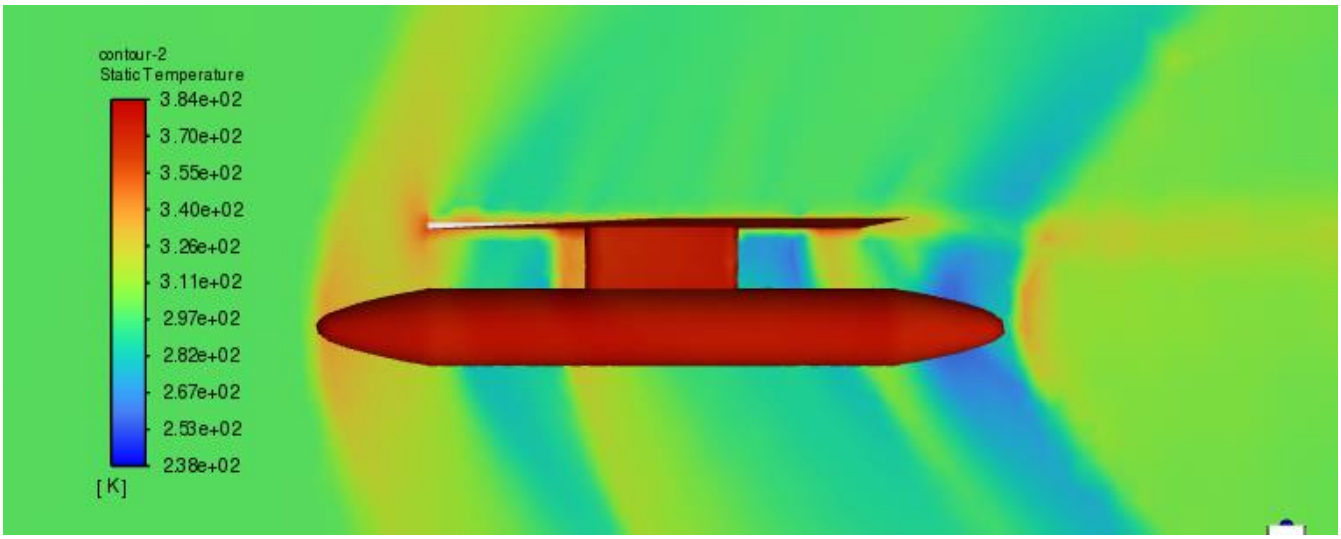

Figure 78: Static Temperature Contour

Forces - Direction Vector (1 0 0)

	Forces [N]			Coefficients		
Zone	Pressure	Viscous	Total	Pressure	Viscous	Total
fuel_tank	28631.613	1438.1017	30069.715	0.06523123	0.0032764183	0.068507648
pylon_	12725.297	151.75816	12877.055	0.028991966	0.0003457497	0.029337716
tube	531.65887	46.586147	578.24502	0.0012112752	0.00010613693	0.0013174121
Net	41888.569	1636.446	43525.015	0.095434471	0.0037283049	0.099162776

Figure 79: Force Result

0.75m Pylon Length Results

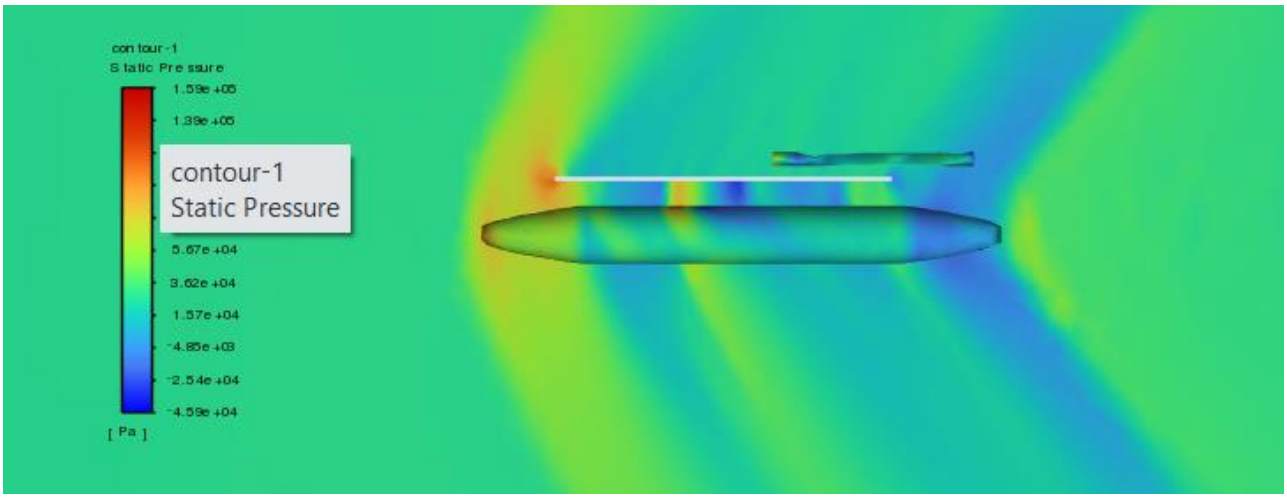

Figure 80: Static Pressure Contour

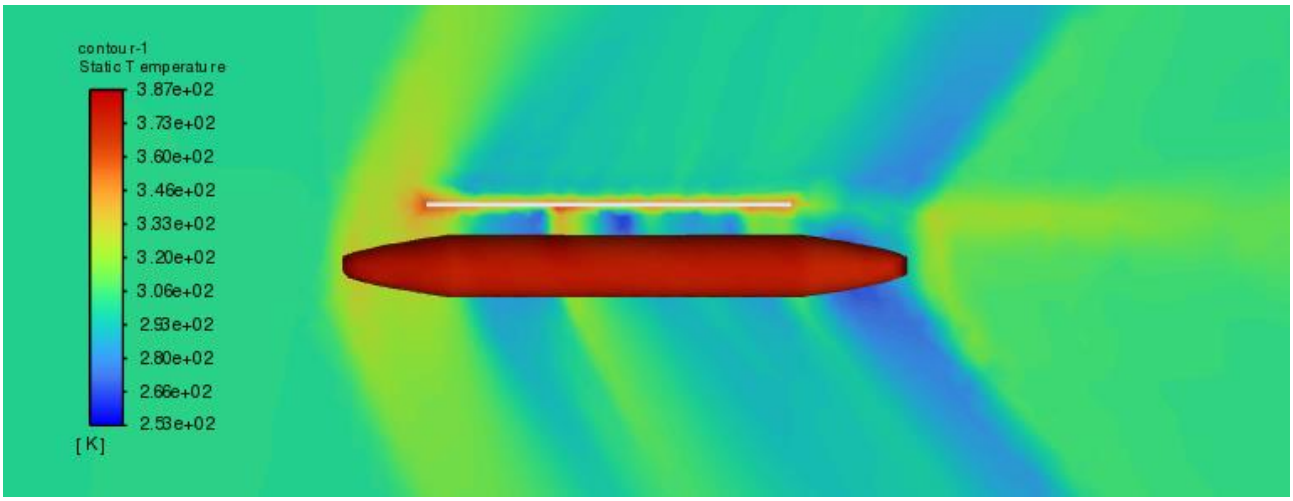

Figure 81: Static Temperature Contour

Forces - Direction Vector (1 0 0)

	Forces [N]			Coefficients		
Zone	Pressure	Viscous	Total	Pressure	Viscous	Total
fuel_tank	27328.082	1267.132	28595.214	0.061708937	0.0028612826	0.064570219
pylon	6964.8813	146229.61	153194.49	0.015727244	0.33019784	0.34592509
repaired_-_wing	39340.93	2360.5537	41701.483	0.088834882	0.0053303141	0.094165196
tube	969.98206	36.265697	1006.2478	0.002190295	8.1890768e-05	0.0022721858
Net	74603.875	149893.56	224497.44	0.16846136	0.33847133	0.50693269

Figure 82: Force Result

0.5 m Pylon Length Result

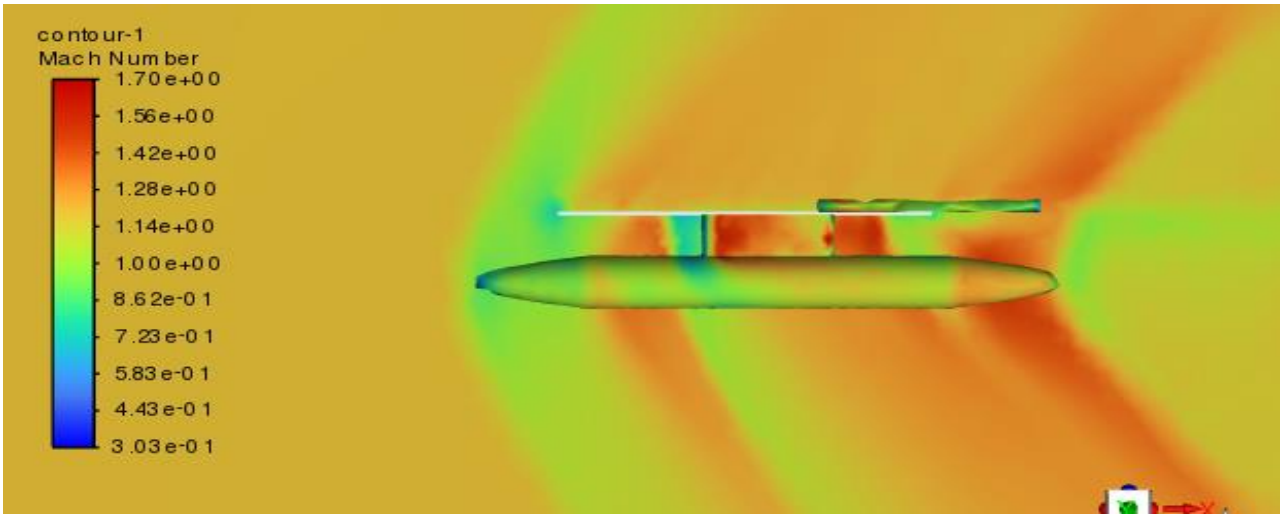

Figure 83: Mach Number Contour

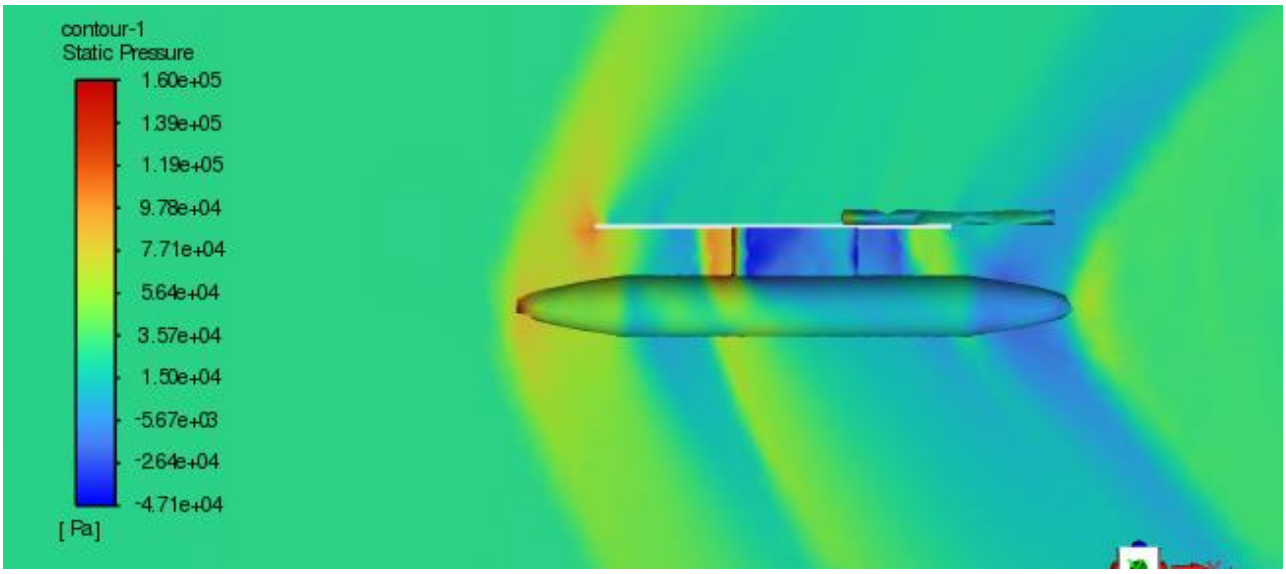

Figure 84: Static Pressure Contour

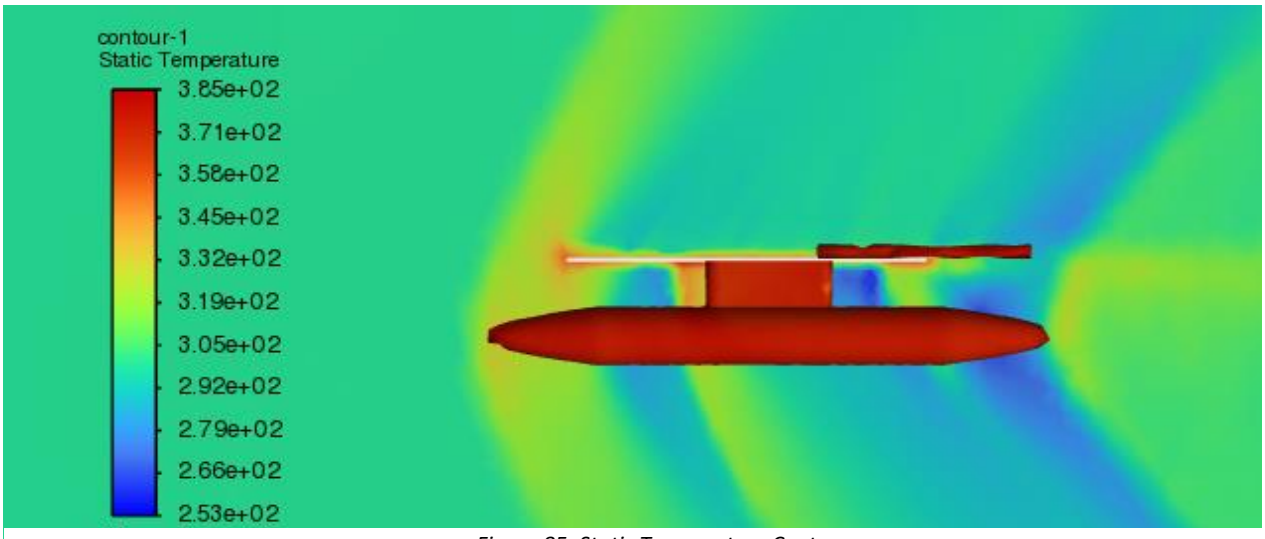

Figure 85: Static Temperature Contour

Forces - Direction Vector (1 0 0)

	Forces [N]			Coefficients		
Zone	Pressure	Viscous	Total	Pressure	Viscous	Total
fuel_tank	27364.318	1291.233	28655.551	0.062343929	0.0029418069	0.065285736
pylon	13112.03	150.37788	13262.408	0.029873044	0.00034260485	0.030215649
repaired_-_tube	3574.1016	42.736309	3616.8379	0.0081428498	9.7365825e-05	0.0082402156
wing	37051.66	147387.22	184438.88	0.08441453	0.33579124	0.42020577
Net	81102.11	148871.57	229973.68	0.18477435	0.33917301	0.52394737

Figure 86: Force Result

0.3m Pylon Length Results

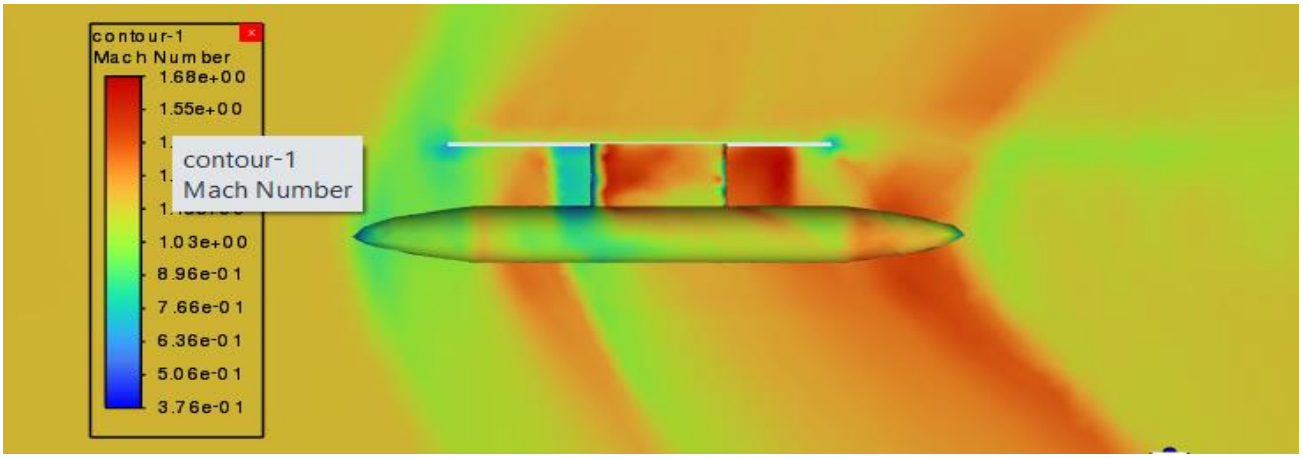

Figure 87: Mach Number Contour

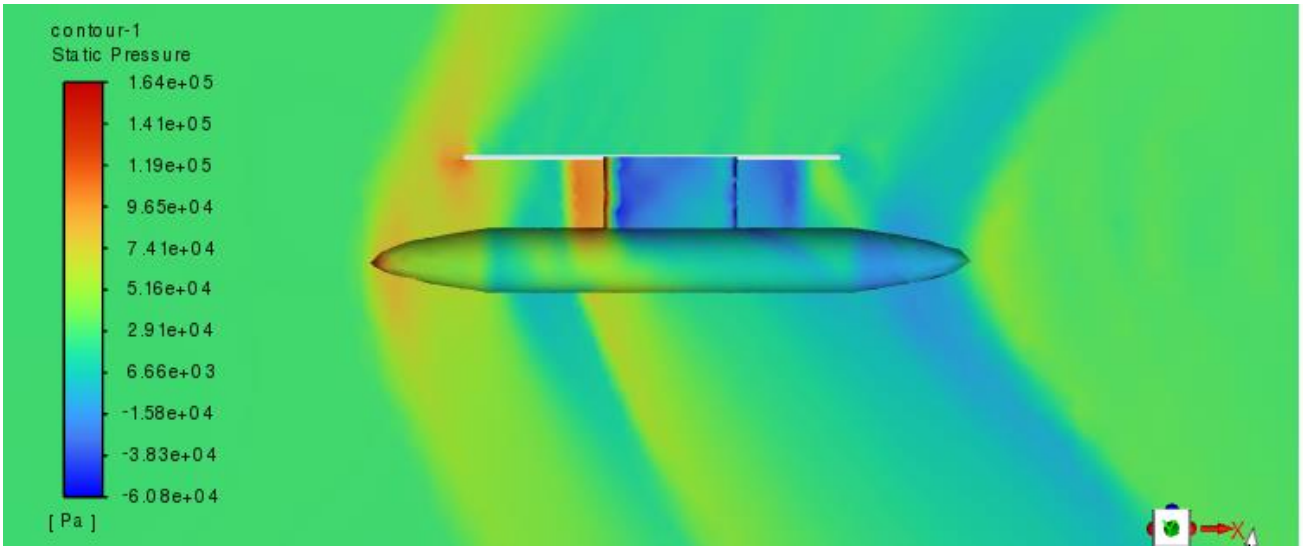

Figure 88: Static Pressure Contour

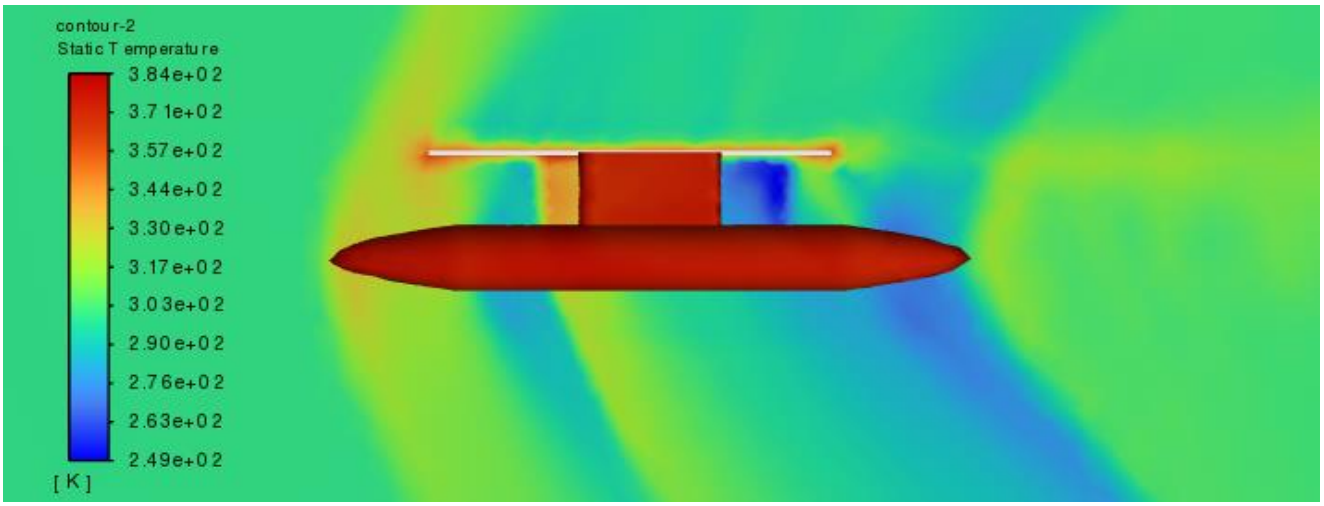

Figure 89: Static Temperature Contour

Forces - Direction Vector (1 0 0)

	Forces [N]			Coefficients		
Zone	Pressure	Viscous	Total	Pressure	Viscous	Total
fuel_tank	26887.92	1287.3857	28175.306	0.060769458	0.0029096239	0.063679082
pylon	19426.572	181.90262	19608.475	0.043906047	0.00041111858	0.044317165
wing	40240.441	151158.98	191399.43	0.090947527	0.34163482	0.43258234
Net	86554.934	152628.27	239183.21	0.19562303	0.34495556	0.54057859

Figure 90: Force Result

Pylon Length (Height)	Drag Coefficient (Cd)
1m Pylon Length	0.0954
0.7m Pylon Length	0.1684
0.5m Pylon Length	0.1847
0.3m Pylon Length	0.1956

In the table, four different pylon lengths were experimented with, and the best result was obtained from the longest pylon. This could be attributed to shock waves, as normally, an increase in length, while maintaining the same width, would lead to increased drag due to a larger surface area.

Based on the conducted analyses, a pylon length of 1 meter is deemed suitable for mounting the 1.2L Power Series Tank. Numerical calculations were performed with Ansys Fluent support.

Conclusion

In summary, the project's goal is to increase the mission duration and range of supersonic fighter jets flying at speeds exceeding the speed of sound. To achieve this, it is crucial to reduce the drag coefficient. Throughout aviation history, engineers have employed various methods to address this challenge. In our case, we turned to shape optimization, focusing on reducing wave drag, the most challenging type of drag under mission conditions.

The approach involved working on nose cone geometries, primarily utilized in rocketry. We adapted these designs to our field and tested two different geometries, namely Haack Series and Power Series, both demonstrating good performance under mission conditions. Following analyses, the Power Series 1.2L fuel tank exhibited the best performance. It can be inferred that longer and generally slender nose cone geometries enhance aerodynamic performance. 6 meters tanks outperformed 4 meters tanks. Additionally, numerical analyses were repeated for the critical pylon length, revealing an unexpected trend: as the pylon length increased, contrary to expectations, the drag coefficient tended to decrease due to wave formation.

In conclusion, the slender and long nose cone with Power Series geometry, along with a 1-meter height pylon, achieved the best performance.

References

1. U.S. Department of Transportation FEDERAL AVIATION ADMINISTRATION, Pilot's Handbook of Aeronautical Knowledge, FAA-H-8083-25B, (2016).
2. Malalasekera, W., & Versteeg, H. K. (2007). An introduction to computational fluid dynamics. The finite volume method, Harlow: Prentice Hall, 1995.
3. CONVERSE, L., LEVENETZ, B., & MAHOOD, L. Variable geometry external fuel tanks. In 12th Structures, Structural Dynamics and Materials Conference (p. 395).
4. Harries S, Practical Shape Optimization Using CFD, Whitepaper, FRIENDSHIP SYSTEMS, (2014).
5. Hu, R., Jameson, A., & Wang, Q. (2012). Adjoint-based aerodynamic optimization of supersonic biplane airfoils. Journal of Aircraft, 49(3), 802-814.
6. Crowell G.A. (1996). The Descriptive Geometry of Nose Cone, Scribd.
7. Ansys Fluent User's Guide, Release 2021 R2, July 2021
8. www.nasa.gov
9. en.wikipedia.org